UNIVERSITAT POLITÈCNICA DE VALÈNCIA

School of Telecommunications Engineering

EVALUATION OF DRY-ETCHING TECHNIQUES FOR FACET FORMATION OF AlGaAs-BASED EDGE-EMITTING LASER DIODES

Master's thesis

Master's Degree in Telecommunication Engineering

AUTHOR: Santiago Cerdà Moreno

Tutor: Felipe Laureano Peñaranda Foix

External cotutor: Ralph-Stephan Unger

ACADEMIC YEAR: 2024-2025

Abstract

In this work, functional GaAs-based laser diodes with etched facets are demonstrated. In order to achieve this, extensive front-end work in the clean room and optoelectronic measurements was carried out. With the aim of obtaining optimal results in facet etching, previous optimization work for the etching recipes in test wafers was completed. Then, a full laser diode production front-end process with epitaxially-structured wafers was followed. Finally, after wafer singulation, the devices were optoelectronically measured to determine their emission spectrum and intrinsic parameters.

Resum

En aquest treball, es demostren diòdes làser funcionals basats en GaAs i amb facetes gravades. Per a aconseguir-ho, s'ha dut terme un extensiu treball de front-end en sala neta i mesures optoelectròniques. Per tal d'obtindre resultats òptims en el gravat de les facetes, primer s'ha completat un treball previ d'optimització de les receptes de gravat en oblies de prova. Seguidament, s'ha seguit un procés complet de front-end per la producció de diòdes làser fent ús d'oblies de GaAs amb estructures epitaxials. Finalment, després de singular els dispositius, aquests han sigut sotmesos a mesures optoelectròniques del seu espectre i paràmetres intrínsics.

Resumen

En este trabajo, se demuestran diodos láser funcionales basados en GaAs y con facetas grabadas. Para conseguirlo, se ha realizado un extensivo trabajo de front-end en sala limpia y medidas optoelectónicas. Con el objetivo de obtener resulados óptimos en el grabado de las facetas, primero se ha completado un trabajo previo de optimización de las recetas de grabado en obleas de prueba. A continuación, se ha seguido un proceso completo de front-end para la producción de diodos láser haciendo uso de obleas de GaAs con estructuras epitaxiales. Finalmente, después de singular los dispositivos, éstos han sido sometidos a medidas optoelectrónicas de su espectro de emisión y parámetros intrínsicos.

Resumen Ejecutivo

La memoria del TFG/TFM *Evaluation of dry-etching techniques for facet formation of AlGaAs-based edge-emitting laser diodes* debe desarrollar en el texto los siguientes conceptos, debidamente justificados y discutidos, centrados en el ámbito de la electrónica y optoelectrónica.

CONCEPT (ABET)	**CONCEPTO (traducción)**	**¿Cumple? (S/N)**	**¿Dónde? (páginas)**
1. IDENTIFY:	1. IDENTIFICAR:		
1.1. Problem statement and opportunity	1.1. Planteamiento del problema y oportunidad	S	1
1.2. Constraints (standards, codes, needs, requirements & specifications)	1.2. Toma en consideración de los condicionantes (normas técnicas y regulación, necesidades, requisitos y especificaciones)	S	1
1.3. Setting of goals	1.3. Establecimiento de objetivos	S	21
2. FORMULATE:	2. FORMULAR:		
2.1. Creative solution generation (analysis)	2.1. Generación de soluciones creativas (análisis)	S	25, 41
2.2. Evaluation of multiple solutions and decision-making (synthesis)	2.2. Evaluación de múltiples soluciones y toma de decisiones (síntesis)	S	30 - 33
3. SOLVE:	3. RESOLVER:		
3.1. Fulfilment of goals	3.1. Evaluación del cumplimiento de objetivos	S	62 - 63
3.2. Overall impact and significance (contributions and practical recommendations)	3.2. Evaluación del impacto global y alcance (contribuciones y recomendaciones prácticas)	S	62 - 64

Contents

1 Introduction..1
2 Fundamentals and Theoretical Framework..2
    2.1 Lasers..2
        2.1.1 Physical Principles...2
        2.1.2 Types of Lasers...3
        2.1.3 Laser Diodes..4
    2.2 Semiconductors..7
        2.2.1 Structures and Crystals...7
        2.2.2 Bandgap and Energy Levels...7
        2.2.3 Indirect Bandgap Semiconductors...9
        2.2.4 Direct Bandgap Semiconductors..9
    2.3 Laser Front-End Processing...13
        2.3.1 Etching Techniques..13
        2.3.2 ICP-RIE..14
        2.3.3 Variables..15
        2.3.4 In-Situ Etch Depth Control...16
    2.4 Thin Film Deposition..17
        2.4.1 Thin Film Deposition Techniques...17
        2.4.2 Chemical Vapor Deposition...18
3 Motivation and Past Work..20
    3.1 State of Art..20
    3.2 Past Work..20
    3.3 Objectives..21
    3.4 Proposal..21
4 Front-end Processing...23
    4.1 Process Overview..23
    4.2 Ridged Waveguide Etching...23
    4.3 Facet Etch with Photoresist..25
    4.4 Facet Etching with Hard Mask..27
    4.5 Results and Discussion..30
    4.6 Full Device Process...33
        4.6.1 K-Layer...36
        4.6.2 I-Layer..38
        4.6.3 M-Layer..39
        4.6.4 K1-Layer...40
        4.6.5 RS-Layer...44
    4.7 Evaluation and Characterization of Devices..45
5 Results and Outlook..48
    5.1 Results...48
        5.1.1 Summary...48

5.1.2 Recipe Optimization.. 48
5.1.3 Laser Performance.. 52
5.1.4 Final Remarks.. 62
5.2 Future Work.. 63
6 References.. 65
7 List of Tables.. 69
8 List of Figures.. 70
9 Abbreviations.. 73
10 Acknowledgements.. 75

1 Introduction

The special properties of gallium arsenide and its derivatives, namely its direct bandgap and high electron mobility, render this compound the most frequently used material for light sources. Gallium arsenide can be employed in the fabrication of numerous devices, such as heterojunction bipolar transistors (HBT), metal-oxide-semiconductor field-effect transistors (MOSFET), or light-emitting diodes (LED).

Although numerous compounds, such as InP or GaN, can be used as platform for the fabrication of these devices depending on wavelength requirements, those based in GaAs present a less complex fabrication process, lower associated costs, and cover other sections of the spectrum.

GaAs-based laser diodes are the most efficient light sources in the semiconductor industry. Their high efficiency, narrow band of emission, and long lifespan are only some of the unique features that allow them to be employed in applications spanning over multiple fields, notably ranging from telecommunications to medicine.

The advantages of GaAs-based photonic devices can be combined with silicon-based driver technologies for heterogeneous integration. This approach, also known as the chiplet process, involves micro-transfer printing (µTP) and requires the etching of the device facets, that is, the perpendicular lateral surface through which the light beam of the laser will be emitted.

The manufacturing of laser diodes based on GaAs requires wafer-level fabrication in the clean room, including the accurate deposition and etching of multiple material layers as well as contacting and device insulation. For the etching of the facet, adequate smoothness and vertical profile angle are of the utmost importance. Whether these requirements are met or not will determine the light output of the devices and they will thus be the main focus of this study.

In this work, functional light-emitting GaAs-based laser diodes with etched facets will be demonstrated, accompanied by their direct comparison to laser diodes with only cleaved facets and to a hybrid configuration. Their performance will be quantitatively analyzed according to emission spectrum, power- and voltage-current characteristics, and farfield emission.

This work will consist of the following structure. First, the physical and chemical principles, processes, and materials relevant to this work will be covered, along with an overview of the current state of art in etched-facet laser devices. Next, a thorough explanation of the front-end practical work to build the laser diodes will follow. Then, the results of the optical measurements will be discussed, focusing on comparing cleaved and etched facets. Finally, an outlook on future work that should enable heterogeneous integration of such laser devices with etched facets will be provided.

2 Fundamentals and Theoretical Framework

2.1 Lasers

2.1.1 Physical Principles

Standing for Light Amplification by Stimulated Emission of Radiation, lasers are devices that produce narrow and intense beams of coherent light. Unlike ordinary light sources that emit light in many wavelengths and directions, lasers emit light coherently (in-phase), directionally (in the form of a narrow beam), and virtually monochromatically (only in an extremely limited wavelength range).

The physical principles of lasers can be tracked back to Albert Einstein, who introduced the concept of stimulated emission - the process through which an incoming photon causes an atom to emit a second photon of the same energy, phase, and direction. This laid the groundwork for the development of lasers throughout the 20th century, namely, with the first ever operational laser based on a ruby crystal by Theodore Maiman in 1960 [1].

In order to understand the working principles of lasers, it is crucial to understand the three processes of light interaction with matter [2]:

- Absorption. Excitation of atoms or molecules in which electrons move from a lower state of energy to a higher one due to incoming photons.
- Stimulated Emission. Release of an additional photon after an excited electron is hit by another incoming photon. The additional photon will share the same properties as the incoming photon, reinforcing the beam of light. This constitutes the critical working principle of lasers.
- Spontaneous Emission. Return of the electrons to their lower energy state after a brief period of time. This process occurs in random time and direction.

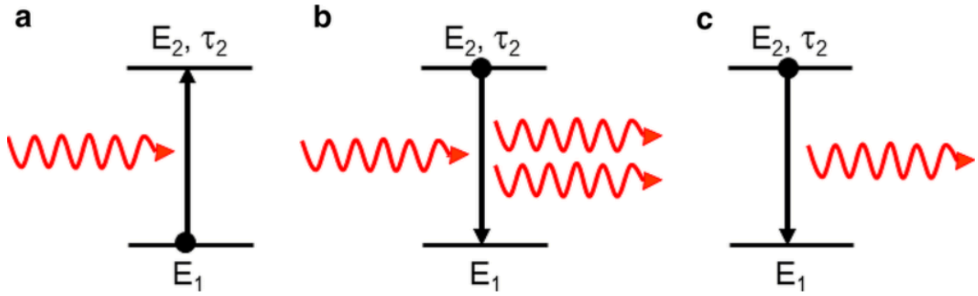

Figure 2.1. Depiction of the a) absorption, b) stimulated emission, and c) spontaneous emission by a two-level atom that presents two energy states E_1 and E_2 with a luminescence lifetime of τ_2.

[1] Pollnau, Markus. (2019). Are absorption and spontaneous or stimulated emission inverse processes? The answer is subtle! Applied Physics B. 125. 10.1007/s00340-019-7133-z.

However, in order to sufficiently sustain the laser process, stimulated emission must dominate over absorption. While in most natural systems electrons tend to stay in the lower energy states, rendering incoming photons more likely to be absorbed, this balance is reversed in laser systems through a process called population inversion.

Population inversion occurs when a majority of the electrons find themselves in an excited state rather than in the ground state. Given that this is not their naturally stable condition, an external energy source or pump must be employed. Once population inversion is achieved, the likelihood of stimulated emission is considerably higher, leading to a chain reaction that amplifies the light beam.

If the gain medium, that is, the active region where population inversion takes place, is placed between two surfaces with their respective reflectivities forming an optical cavity, the photons will reflect back and forth, triggering further stimulated emissions, amplifying light in a coherent manner, and allowing it to escape in the form of a narrow laser beam.

2.1.2 Types of Lasers

Depending on the gain medium, operating mode, or output characteristics, there are different categories of lasers suited to specific applications. Following the most common classification, which is based on gain medium, it is widely accepted that lasers can be divided in five big families [3]:

- Solid-state Lasers. Using a solid crystalline or glass material doped with rare-earth ions (Nd, Ed), solid-state lasers present a high output power and remarkable efficiency. Ruby, garnet, Ti:sapphire, or Nd:YAG lasers are the main examples of solid-state lasers.

- Gas Lasers. Gas lasers make use of an electrical current that passes through a gas or mixture of gases to excite atoms and achieve population inversion. Employing CO_2, He-Ne mixes, or mixtures of halogens and noble gases, such as KrF, ArF), they diverge in efficiency, power output, and emitted wavelengths, ranging from infrared to ultraviolet. While they produce very stable beams and present longer lifespans than solid-state lasers, they often also require more complex cooling and gas circulation systems.

- Fiber Lasers. Often included in the solid-state category, fiber lasers use optical fibers (silica glass) mixed with rare-earth elements (Yt, Er). The special light guiding properties of optical fibers is what turn fiber lasers into their own family, offering smaller, straighter and more precise beams at low maintenance and operating costs.

- Liquid Lasers. Also known as dye lasers, liquid lasers use organic dyes dissolved in a solvent as the gain medium to then be pumped by another laser or flash pump. Depending on the employed dye, these lasers can be tuned across a wide range of wavelengths, which makes them fit for applications where this feature is needed. Nonetheless, they require a complex setup for dye circulation, which leads to difficult maintenance demands.

- Semiconductor Lasers. Based on p-n junctions, semiconductor lasers (most of them also known as diode lasers) are compact, efficient, and widely used. They can range from infrared to visible light depending on the semiconductor material (GaAs, GaN, InP). Semiconductor lasers are very frequently arrayed to increase the total power output and used as energy sources to pump other kinds of lasers. They are regarded as the light source with the highest efficiency.

Given the applications that we are aiming for - integrated elements for optoelectronic and photonic devices - laser diodes are the most suitable in our case. We will now go into further detail on their structure and physical principles.

2.1.3 Laser Diodes

Laser diodes or semiconductor lasers are compact and efficient light sources that emit coherent radiation through the process of stimulated emission, following the previously explained physics. They are vital components in a wide range of applications, such as fiber-optic systems, photonic integrated circuits, and quantum platforms. Laser diodes combine the functionality of electronic and photonic components, offering high-speed modulation and miniaturization possibilities.

Their structure consists of a p-n junction, as found in regular diodes, embedded within a double heterostructure that confines both carriers and photons. Its major components can generally be divided into [4]:

- Electrical Contacts: Metal contacts are deposited on the p-type and n-type regions in order to inject current through the p-n junction.
- Cladding Layers: Part of the P-N junction, these layers present a lower refractive index to achieve light confinement.
- Waveguide layers: Also part of the P-N junction and enclosing the active zone, they are composed of multiple sub-layers with distinct refractive indexes that guide the light.
- Active Zone: Central region where carrier (electron-hole) recombination takes place resulting in photon generation. It is often formed making use of narrow bandgap materials (GaAs, InGaAsP) stacked between higher-bandgap materials for carrier and optical confinement.

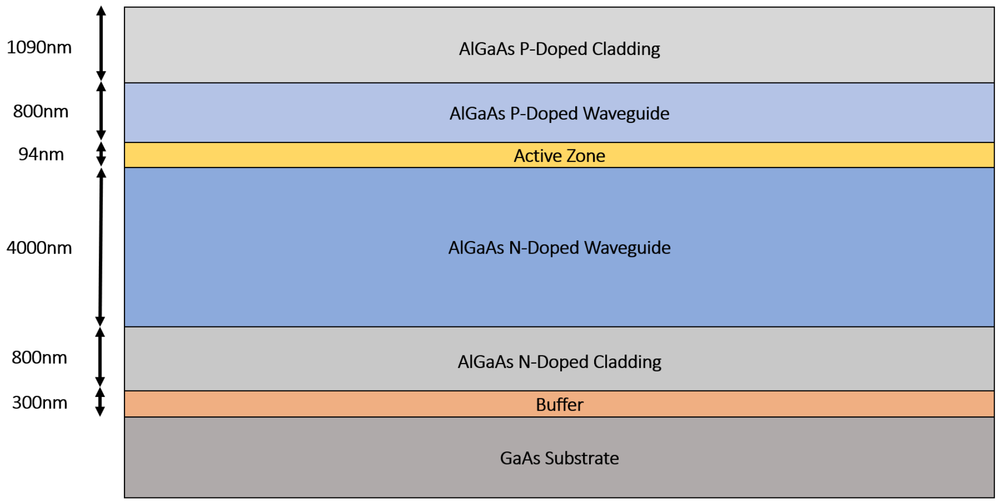

Figure 2.2. Schematic of the laser epitaxy of the wafers.

As it will later be explained, these layers are epitaxially grown from the substrate using metal-organic vapor phase epitaxy in a vertical manner to ensure a constant crystal lattice is kept. Only epitaxially grown structures are of sufficient crystalline quality to allow for lasing capabilities. If they were not grown this way, the defects and interfaces between layers would result in non-radiative recombination, which would lead to heat dissipation instead of light emission.

Moreover, in order for the light to be guided in the right direction and for the modes to be correctly confined, the presence of a ridge waveguide (RWG) is needed. Consisting of a small raised strip etched on top of the device, the RWG creates a lateral refractive index difference that forces light to be confined under the ridge. The light is therefore confined in two directions:

- Vertical confinement. The active layer has a higher refractive index than the layers above in below it.
- Horizontal confinement. The lateral refractive index contrast created by the RWG causes the light to stay under the ridge and not spread sideways.

The cavity also has to be limited at the ends to trap the light. If the limits of the cavity are limited by facets that reflect the photons and only allow a small of light to escape, a Fabry-Pérot cavity is formed, like in our case. Other configurations make use of Bragg grating to trap only photons with a specific wavelength.

As discussed, stimulated emission, population inversion, and optical feedback enable the devices to maintain constant photon emission. Photons emitted in the active region are confined in the optical cavity, in which resonance occurs at discrete modes satisfying the cavity condition:

$$L = \frac{m \cdot \lambda}{2 \cdot n}$$

where L is the cavity length, λ is the lasing frequency, n is the refractive index, and m is an integer mode number [2]. Only photons that match this condition will form the emitted light beam.

Additionally, several other physical and material parameters also determine the behavior and efficiency of laser diodes [5]:

- Quantum Efficiency (η_i, η_e): While the internal quantum efficiency (η_i) is given by the ratio of generated photons over electron-hole pair recombination, external quantum efficiency (η_e) considers losses and coupling inefficiencies.

- Threshold Current (I_{th}): The threshold current is the minimum injection current at which the gain equals the cavity loss and lasing starts. It depends on numerous parameters such as temperature, cavity length, reflectivity, and material purity. Lower threshold currents are desired for efficiency.

$$I_{th} = A \cdot J_{th} = A \cdot J_{tr} \bullet e^{\left(\frac{1}{g_0 \Gamma}\left[\alpha_i + \frac{1}{2L} ln\left(\frac{1}{R_1 R_2}\right)\right]\right)}$$

where J_{tr} is the transparent current density, g_0 is the differential gain coefficient, Γ is the optical confinement factor, α_i is the internal loss coefficient, and R_1 and R_2 are the reflectivities of the facets. The reflectivity of a facet, which in the case of GaAs to air facets is of 30%, can be described by the refractive index of the semiconductor (n_s) and that of the ambient (n_0):

$$R = \left(\frac{n_s - n_0}{n_s + n_0}\right)^2$$

- Slope Efficiency (η_s): Rate at which the output optical power increases with above threshold current. It depends on quantum and coupling efficiency as well as optical losses, which are related to the reflectivity of the cavity and therefore their profile angle.

$$\eta_S = \frac{dPout}{dI} = \frac{\hbar\omega}{e} \bullet \eta_i \bullet \frac{\frac{1}{L} ln \frac{1}{R_1 R_2}}{\alpha_i + \frac{1}{2L} ln \frac{1}{R_1 R_2}}$$

After getting a general grasp of the physical principles of laser diodes and discover what variables will affect the final performance of the future devices, we will now cover the steps of wafer-based cleanroom work that will be later performed.

2.2 SEMICONDUCTORS

2.2.1 Structures and Crystals

Semiconductors are fundamental in both photonics and electronics. The fact that their electrical conductivity lies between that of conductors and insulators enables them to be modulated by different variables such as doping concentration, temperature or electromagnetic fields. This tunability renders semiconductors the cornerstone of multiple active devices, ranging from diodes and transistors to sensors and lasers. [6]

Regarding their structure, most technologically relevant semiconductors present covalently bonded crystals in the form of periodic lattices. Elemental semiconductors, for instance Si and Ge, crystallize in diamond cubic structures, whereas compound semiconductors belonging to the III-V group of the periodic table typically present a so-called zinc blende structure, showing a certain resemblance to the diamond lattice [7].

The three-dimensional atomic ordering directly impacts their electronic band structure, determining crucial properties such as carrier mobility, effective mass, and most importantly bandgap energy. Crystal symmetry, interatomic forces, or lattice constants also play an important role in shaping the nature of the optical transitions and electronic dispersion relations.

2.2.2 Bandgap and Energy Levels

As we know from solid state physics, the allowed energy states of electrons in a crystal form continuous bands separated by a forbidden energy range known as bandgap. While the valence band contains the electrons with a strong binding to the atomic core, the conduction band comprises the states where an electron is excited and consequently able to move freely, resulting in current conduction.

Taking these two definitions into account, the bandgap energy can be defined as the difference between the highest occupied state in the valence band and the lowest unoccupied state in the conduction band. The bandgap energy therefore determines the fundamental electrical and optical behavior of a material.

According to their crystal momentum, the bandgap of a given material can be categorized in the two following groups [6]:

- Direct bandgap: The valence band maximum and conduction band minimum are located at the same value of crystal momentum. Since this allows electron transitions to conserve momentum, absorption and photon emission in this case are highly efficient.

- Indirect bandgap: The valence band maximum and the conduction band minimum occur at different points in the momentum space. In this case, electron transitions will require a phonon, the quasiparticle representing the elemental unit of vibration, to conserve momentum, which will lower drastically the likelihood of successful radiative recombination.

In figure 2.3, direct and indirect bandgaps are compared in the k-space, that is, the representation of the electron state in relation to their crystal momentum. The Fermi level (e_F), that is, the highest energy value occupied by electrons at 0K, and the Fermi wave number (k_F), the wave number value corresponding to the Fermi level, are both illustrated. In semiconductors, the Fermi level is situated between the conduction and valence band and it is at the Fermi wave number value that bands can be aligned (direct semiconductors) or not (indirect semiconductors).

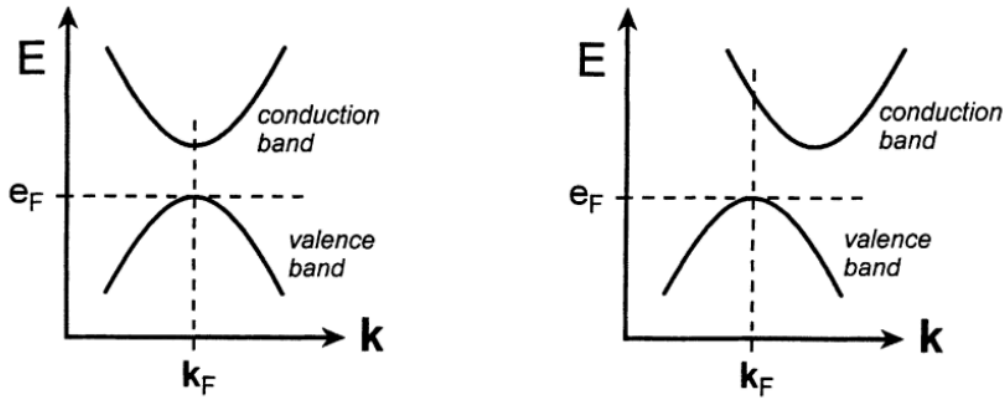

Figure 2.3. Direct bandgap vs. indirect bandgap schemes in the k-space with a given Fermi level (e_F) and wave number (k_F).

[2] Abedin, Minhaz. (2015). A self-adjusting lin-log active pixel for wide dynamic range CMOS image sensor. 10.13140/RG.2.1.3871.8965.

This crucial distinction will determine what material is suited for each application. While direct bandgap semiconductors are best suited for light-emitting devices as previously discussed, indirect bandgap materials are typically used in digital electronics and power applications. We will now go into further detail about these two kinds of semiconductors [6].

2.2.3 Indirect Bandgap Semiconductors

As it is widely known, silicon is by a large margin the most used semiconductor in the industry mainly due to its natural abundance and mature processing technology. Despite its limitations when it comes to optoelectronics, silicon's favorable material properties and economic viability have made it the main platform for microelectronics, found in ICs, microprocessors, and memory devices [8].

The indirect bandgap nature of silicon lies in the fact that its valence band maximum is located at the center, also known as the Γ-point, of the Brillouin zone, that is, the repeating unit that describes the wave-like properties of a crystal in the momentum space, while its conduction band minimum can be found near the X-point along the <100> crystallographic direction. This spatial separation in the momentum space (k-space) leads to an indirect bandgap with approximately 1.12eV of energy value at room temperature [6].

The most obvious consequence of this is the need for an additional phonon to allow for electron transitions between the valence and conduction bands, converting a two-particle interaction into a three-particle one and thereby reducing significantly the probability of radiative recombination, leading to a decrease in photoluminescence efficiency.

Silicon's indirect bandgap nature presents profound implications, both positive and negative:

- Poor optical emission due to its high inefficiency, rendering it unsuitable for light-emitting devices.
- Well-understood and reliable carrier mobility and control, ideal for digital switching and analog circuit design.
- Excellent thermal conductivity and stability, which are critical for heat dissipation in dense integrated circuits.

Although its limitations for optoelectronics are obvious, silicon remains unrivalled in terms of processing maturity. Innovative strategies in material engineering and photonic integration continue to expand silicon and other indirect bandgap semiconductors, such as Ge, beyond their traditional domain [9] [10].

2.2.4 Direct Bandgap Semiconductors

Direct bandgap semiconductors take on a central role in optoelectronics due to their efficiency emitting and absorbing light. Unlike in silicon and other indirect bandgap materials, in which additional phonon participation is needed, in direct bandgap semiconductors the conduction band minimum and the valence band maximum are aligned in the k-space close to the Γ-point, allowing for highly efficient radiative recombination.

Light emitting diodes, photodetectors, solar cells, and, most importantly for this work, laser diodes make use of direct bandgap materials for its production. Among the family of direct bandgap semiconductors, indium phosphide (InP), gallium nitride (GaN), or gallium arsenide (GaAs) and its compounds (e.g., AlGaAs, InGaAs) are the most widely studied and commercially successful elements, all belonging to the III-V family.

Depending on the application, III-V semiconductors can cover a wide range of the optical spectrum when used as the active zone material [4][11]:

Material	Emission Range (nm)	Region	Applications
GaN /InGaN	370 - 530	UV → Blue → Green	Displays, biomedical
InGaP	630 - 690	Orange → Red	Barcode scanners, DVD, displays
GaAs	630 - 1200	Red → Near IR	IR sensors
InGaAs / InGaAsP	1000 - 1650	Near IR	Fiber-optic communication
InAs / InAsSb /PbSe	2000 - 4000	Mid IR	Gas sensing

Table 1. III-V compounds used for laser diodes and their applications.

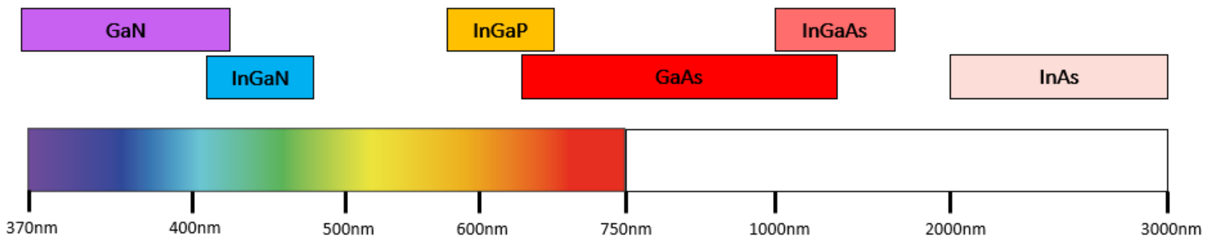

Figure 2.4. Emission spectrum of laser diodes based on different III-V compounds.

Additionally, three of these III-V compounds can be used as the platform in laser diode manufacturing. Each requiring completely different processing steps and equipment, the most frequently used substrates for this purpose are: InP, GaN, and GaAs.

InP

Indium phosphide presents a direct bandgap of approximately 1.34eV and enabled light emission around 920nm when used alone and in the telecommunications window from 1.3µm to 1.6µm as the InGaAsP quaternary alloy. At 1550nm, the loss minimum for fiber optic transmission is found and thus InGaAsP is the ideal semiconductor for these applications.

InP-based photonic integrated circuits (PICs) are frequently found in the industry thanks to their capacity of optical integration of functions, such as lasers, modulators, or detectors, on a single chip. Their low nonlinearities and intrinsic electro-optic modulation also render them ideal for coherent transceivers in dense wavelength-division multiplexing [12].

Higher thermal conductivity also constitutes one of the main advantages of using InP, supporting high output power in lasers, even though the high temperature often needed for its etching and processing present challenges that must be overcome. Nonetheless, InP still remains the material of choice when it comes to wavelength-division multiplexing [13] and recent LiDAR systems [14].

GaN

Another relevant III-V compound is gallium nitride (GaN), presenting a direct bandgap of ~3.4 eV, which corresponds to ultraviolet and visible blue light emission. Two different crystallizations of the compounds can be found, zinc-blende and wurtzite, of which the latter is most frequently used due to its thermo-dynamical stability.

The breakthrough of GaN epitaxy led to the development of efficient blue and purple LEDs, which had been a massive challenge in the past that was not overcome until the 1990s. Revolutionizing solid-state lighting, GaN-based light sources are the main power source for display backlighting and automotive lighting, presenting longer lifetime and higher efficiency than traditional incandescent bulbs.

GaN is also at the forefront regarding high-power RF and power electroncs, with GaN-on-SiC HEMTs [15] being widely used for 5G and satellite communications as well as radar systems. In addition, GaN inherent resistance to high temperatures and radiation damage makes it suitable for extreme environments [16].

GaAs

The final main semiconductor with high relevance in the industry is gallium arsenide (GaAs). Also belonging to the III-V family, its unique physical and electrical properties make it particularly suitable in microwave applications. GaAs presents a direct bandgap of 1.42 eV at room temperature, which, as in the case of the aforementioned semiconductors, make it ideal for optoelectronic devices.

GaAs high electron mobility is approximately five times that of silicon, which is crucial for microwave and millimeter-wave applications, including satellite communications and radar systems. Its remarkable resistance to radiation also renders it a preferred choice for space electronics and military systems.

In order to further enhance and take advantage of the properties of GaAs, numerous alloys and derivatives of gallium arsenide have been developed, incorporating other elements to the compound. Some of the most frequent additions to the compound are Al, resulting in the AlGaAs, or In, leading to the InGaAs, in all of which the percentage of the added material plays a substantial role in its properties, namely its reflective index.

AlGaAs is especially valuable due to bandgap engineering, where the bandgap of the material can be finely tuned by adjusting the ratio of aluminum to gallium. This tunability is crucial in the fabrication of heterojunction devices, where layers of materials with different bandgaps are stacked onto one another in order to control charge carrier behavior. For instance, heterojunction bipolar transistors (HBTs) [17] and high electron mobility transistors (HEMTs) [18] often use GaAs or AlGaAs structures to achieve better light guiding or tune the emission wavelength.

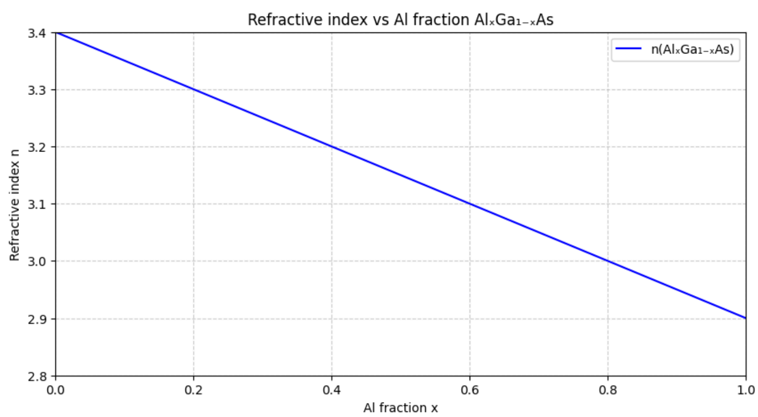

Figure 2.5. Variation of the refractive index of $Al_xGa_{1-x}As$ vs. the fraction of Al(x).

2.3 Laser Front-End Processing

2.3.1 Etching Techniques

In the semiconductor industry, a plethora of physical and chemical processes can be performed in order to pattern and define the nanometric scale structures that are requires for the devices. Ranging from deposition to ion implantation or lithography, the wide range of available techniques performed to our wafers is immense. However, the main process involved in facet laser formation is etching.

Etching is the process through which materials are selectively removed from a substrate usually making use of previous lithography steps, resulting in three-dimensional patterns on layers of materials such as metals, oxides, nitrides, or metals.

Depending on whether the materials are etched away in all directions or only in one, usually vertically, etching processes can be classified in isotropic or anisotropic etching respectively [19]. While anisotropic etching is frequently the preferred option in modern microelectronics for pattern definition, isotropic etching can be interesting to counteract etching defects or selectively etch certain layers.

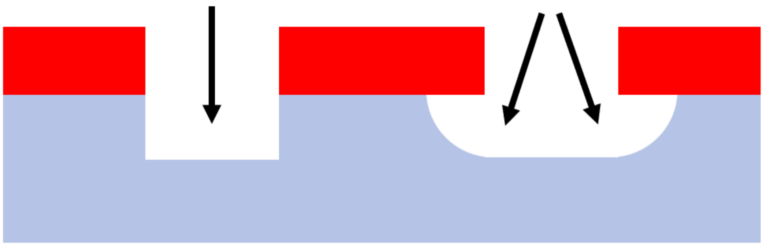

Figure 2.6. Profile shape of anisotropic etching (to the left) vs. isotropic etching (to the right).

Additionally, etching processes can also be split into two main categories based on their focus on chemical or physical components. On the one hand, wet etching uses liquid chemical baths that etch away the desired material in all directions, that is, isotropically, and offers lower costs at the expense of weaker control. On the other hand, dry etching techniques employ gases in plasma states that allow for more control and precise anisotropic patterning [20].

For instance, basic plasma etching is frequently used in simple processes, where plasma generated with radiofrequency powers produce reactive species (ions and radicals) which interact with the exposed surface, leading to volatile products that are etched away. The result is low-damage and isotropic etching.

Moreover, the process can also be carried out by using a configuration consisting of a parallel-plate RF plasma system that generates a DC bias and forces the ions to sputter into the surface. This widely chosen option, known as Reactive Ion Etching (RIE), offers tunable anisotropy and balance between etch rates and selectivity, along with the trade-off of possibly higher damage [21].

2.3.2 ICP-RIE

Ultimately, both techniques can be combined in the so-called Inductively-Coupled Plasma Reactive Ion Etching (ICP-RIE), which presents the most complete tunability options. Making use of two RF sources, one to generate a dense plasma with a coil and the other to apply a DC bias, ICP-RIE allows for independent control of the plasma density and ion bombardment [19].

When compared to regular reactive ion etching, ICP-RIE presents much higher plasma densities, higher aspect ratios through deeper etchings, and better control of sidewall profile and anisotropy, which will be later crucial for our work. Even though the required equipment by the process can escalate into higher costs, it is the preferred option for complex applications where control of the aforementioned variables is of the utmost importance [21].

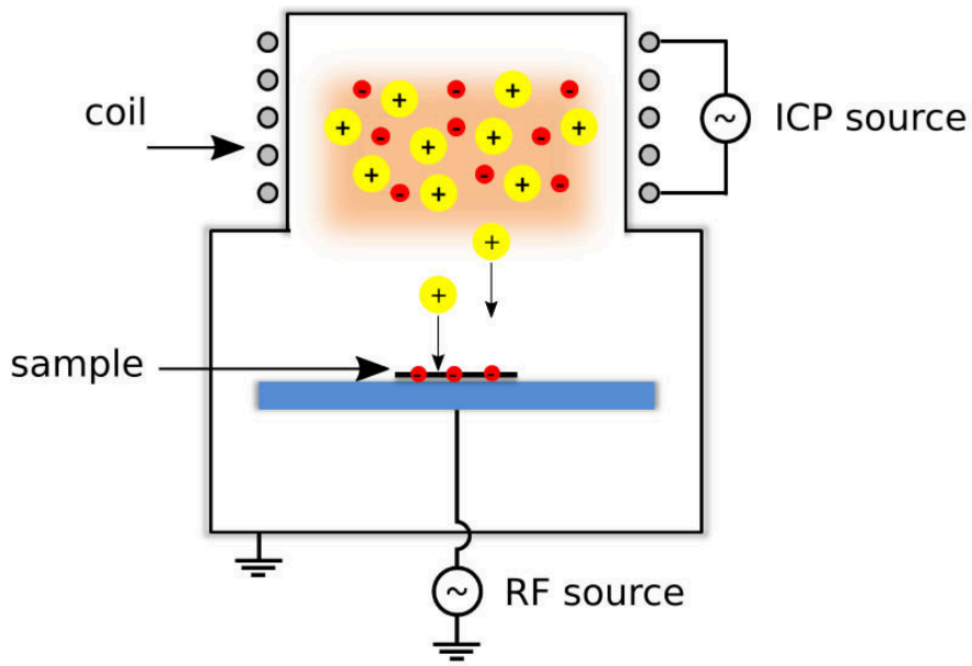

Figure 2.7. Schematics of an ICP-RIE equipment.

[3] Abedin, Minhaz. (2015). A self-adjusting lin-log active pixel for wide dynamic range CMOS image sensor. 10.13140/RG.2.1.3871.8965.

Processes based on multiple chemistries can be performed with such an equipment. For oxides and nitrides, combinations of CHF_3 or CF_4 are frequently used, and when it comes to GaAs-based materials, BCl_3/Cl_2 chemistries are preferred, as in our case. Another widely used process in the industry that employs this technology is the Bosch process, which alternates between SF_6 (etching) and C_4F_8 (passivation) and is used for silicon trench deep etching [20].

2.3.3 Variables

As it has been explained, ICP-RIE is a highly tunable and controllable dry-etching technique that makes use of both physical sputtering and chemical reactions to remove material from a substrate surface. Variables, such as power, pressure or the composition of the gas mix play an essential role in determining the ultimate result of the etching, altering the etch rate, selectivity, aspect ratio, anisotropy, or surface quality, to name a few.

Power

In the ICP-RIE scheme, it must be taken into account that two different power sources are employed: the primary ICP source, that modulates the plasma density, and the RF bias power, which controls the directivity of ion bombardment on the surface. Depending on the desired result, the sources can be tuned so that we obtain a chemistry-dominated isotropic etching through higher ICP power or a sputter-dominated anisotropic etching in which RF power is the focus [22].

Pressure

Determining the ideal pressure of the process is another crucial step to obtain an adequate etching. While lower pressures provide longer mean free paths which allows for high-energy and directional ions to arrive at the surface promoting anisotropic etching, higher pressure causes more ion and radical collisions leading to a higher number of chemical reactions and thus a more chemically-driven etching. [22]

Higher pressure also comes along with potential sidewall erosion due to the higher concentration of etching agents. It is often desired to use low pressures to obtain deeper vertical features and slightly higher pressures in surface with less topology and structure density, where sidewall control is less critical.

Gas Mix

The composition of the gas mix is perhaps the most decisive variable when performing an etching process. Given the wide range of gases to be used, a plethora of gases and different elements can be mixed to enhance an aspect of the etching. Most frequently, both reactive gases and dilution or inert gases are included in the gas mix.

On the one hand, reactive gases, such as BCl_3, Cl_2, CHF_3 or SF_6, supply chemically active species that will form volatile compounds with the substrate material. On the other hand, inert gases, namely He or Ar, are often added to control ion density and enhance physical sputtering, given that they do not partake in the chemical reaction but increase ion bombardment. [23]

Consequently, balancing chemical and physical components is critical to obtain the desired etching behavior. Cyclical flows combining multiple steps with different gas mixes can be carried out for applications where a higher aspect ratio or sidewall passivation are necessary. Additional effects like redeposition or polymerization can also take place under certain chemistries and might require further processing to reduce their negative influence. [24]

2.3.4 In-Situ Etch Depth Control

The etching tools used in the project are equipped with different in situ measurement systems, which are mounted on top of the ICP and RIE etchers to measure the reflected intensity while etching through the epitaxial layers. These tools, which make use of the refraction periods of materials in an epitaxial structure, offer clear depictions of the measurable refraction change as the etching takes place.

Simulating software is also combined to obtain a prediction of what the etch will look like in terms of refractivity periods. The etching simulation software predicts the evolution of depth, profile angle, and roughness based on kinetical, physical and chemical models, which take into account variables such as ion flux, radical flux, ion energy, incidence angle or temperature.

The user provides the required information on the epitaxial structure about to be etched, namely, the refractive indices, absorption coefficients and thickness of each layer, among others, and the software will compute how many refraction periods at a certain wavelength the etching step will last until the value of thickness introduced by the user is reached.

Through comparing the period simulation to the actual measurements coming from the monitoring device in the etcher, the etching becomes highly trackable and can be stopped when desired to meet the requirements and desired depth. The tool used in this work was Multi Layer Simulation V1.3.

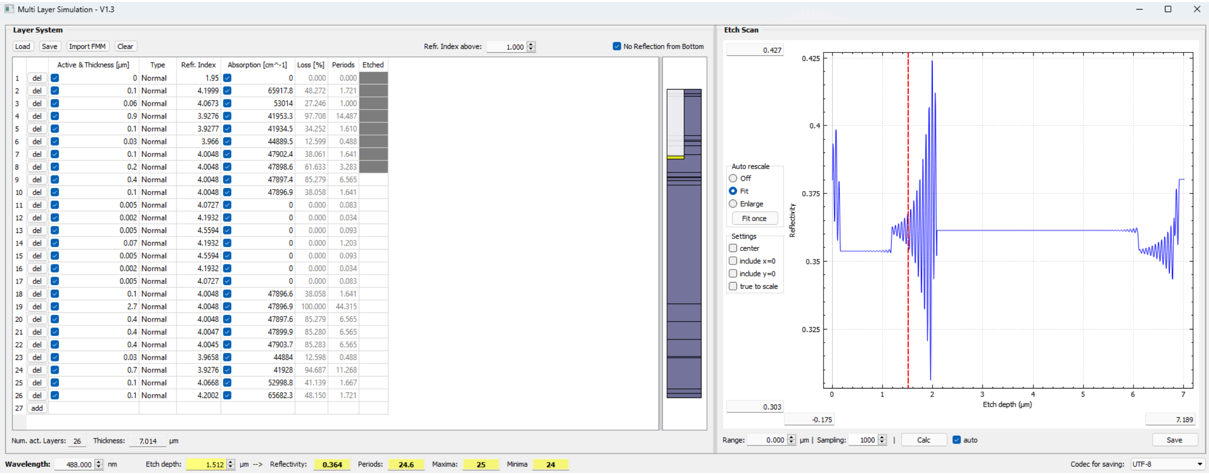

Figure 2.8. View of the simulation software tool for computing refractivity periods. Epitaxial structure of the wafers to the left and the period representation to the right.

2.4 Thin Film Deposition

2.4.1 Thin Film Deposition Techniques

Along with the etching of materials to engrave patterns, the deposition of thin material layers, whether for insulation purposes or to then be partially etched away, is crucial too. Thin films, composed of materials and ranging from nanometers to several micrometers in thickness, are essential in semiconductor processing and production, given the ability to tune their optical, chemical and mechanical properties of a substrate, allowing for new and improved functionalities [25].

Deposition techniques broadly fall into two main categories, namely physical or chemical, depending on the main component that adds to the deposition. While physical methods deposit material in vapor form with little to no chemical reactions taking place on the surface of the substrate, chemical methods rely on these very chemical reactions at or near the surface to form the desired thin layer of material. Given the techniques used in this work, the focus will be laid on chemical techniques.

When it comes to chemical thin layer deposition processes, the two main employed techniques in the industry are Chemical Vapor Deposition (CVD) and Atomic Layer Deposition (ALD). In this work, the focus will be put on CVD.

2.4.2 Chemical Vapor Deposition

Chemical Vapor Deposition, along with all its derivative processes, has been the preferred option and the standard in the semiconductor industry for decades. Involving the introduction of volatile precursor compounds into a reaction chamber containing the heated surface, precursor molecules are adsorbed onto the substrate, chemically reacting with it and thus forming a thin solid film. Multiple reaction can take place, ranging from reduction or oxidation to decomposition. Additionally, gaseous byproducts are simultaneously evacuated from the chamber [25].

Thanks to the vast range of available precursors, chemical vapor deposition allows for strong control over film composition and also deposition of more complex or even three-dimensional structures [11].

The process sequence of chemical vapor deposition is as follows:

1. Precursor introduction. Precursors in the gas state are introduced, often accompanied by H_2 or N_2 molecules or inert gases such as Ar.
2. Transport to substrate. These materials are then directed to the substrate via convection and diffusion within the reactor.
3. Surface reaction. Adsorption and chemical transformation take place on the hot surface of the substrate.
4. Byproduct removal. Volatile species desorb and are evacuated from the chamber.

The main chemical vapor deposition process can be further modified by one or multiple variables in order to suit and serve for specific purposes or applications. The two modalities that were employed in the manufacturing of the laser diodes were:

- Plasma Enhanced Chemical Vapor Deposition (PECVD). This modality of CVD uses plasma for reactive radical and ion generation, with energetic electrons being those who provide the necessary activation energy instead of thermal energy, which also lowers the required substrate temperature, roaming around 150°C to 400°C [11]. Even though it offers a high tunability by modifying the plasma parameters, there is a chance of ion damage and need for post-deposition treatment. Dielectric layers in integrated circuits or passivation layers in solar cells are frequently achieved through PECVD. In this work, this technique was used for Si_3N_4 deposition.
- Metal-organic Chemical Vapor Deposition (MOCVD). Also known as Metal-Organic Vapor Phase Epitaxy (MOVPE), MOCVD makes use of gaseous precursors, namely metal-organic compounds, that decompose when the substrate is heated up to 600-800° through pyrolytic reactions [6]. It offers high throughput and allows for the growth of complex structures, such as quantum wells or DFBs. It is the industry standard for laser epitaxial growth and it was used to epitaxially grow the wafers that were used in this work. The typical reaction used for GaAs growth is as follows:

$$AsH_3 + Ga(CH_3)_3 \rightarrow GaAs + 3\ CH_4$$

The byproducts of the reaction must form stable metalorganic compounds that can then be evacuated from the reactor.

Other variations of chemical vapor deposition, such as Low Pressure Chemical Vapor Deposition (LPCVD) or atmospheric pressure chemical vapor deposition (APCVD), cater to specific needs in some semiconductor manufacturing processes [25].

3 Motivation and Past Work

3.1 State of Art

Taking a dive into the state of art of laser diodes with etched facets, a lot of progress has been achieved in recent years. The etching of the facets has been and still is a delicate aspect of process. Undesired defects, poor profile angles, or excessive roughness are likely to appear and can strongly hinder the device performance by influencing the facet's reflectivity and therefore the intrinsic characteristics of the device, as previously explained.

The main step in facet formation consists of a dry-etching process, which will not offer completely vertical facets. An additional wet-etching step after the main dry-etching process using hydroxides such as TMAH can help obtaining more vertical walls, driving profile angles close to 90° [26].

Moreover, etched facets allow for heterogeneous integration, making them necessary in many photonic integrated circuit applications. The development of laser processes that allow for micro-transfer printing (MTP) of devices into other platforms, such as silicon-based photonics, is one of the main focus of research in the field. Even though this technology offers low costs and eases scalability, there is plenty of research still to carry out regarding coupling efficiency and manufacturing [27].

Laser diodes with etched facets based on other III-V compounds have already been proved successful. GaN-based Fabry-Pérot laser diodes offering up to 28mW at low injection currents have been demonstrated [28] and InP-based laser diodes with high internal efficiency have been achieved too [29].

3.2 Past Work

The optoelectronics department at the Ferdinand Braun Institut has already made a lot of progress in the direction of the contents of this work, that is, the completion of functional diode lasers with reduced device dimensions and high power. So far, a safer but more complex version of the process that will be proposed hereinafter has been carried out using AlInGaP waveguides and AlInP claddings in order to obtain such devices.

The process is divided in multiple layers:

- K-Layer: Contains the ridged waveguides and determines the direction and length of the devices.
- K1-Layer: Determines the location of the facet trenches.

- I-Layer: Describes the regions that will be covered by an insulting layer to isolate them from external disturbances. The facet area and contacts are left exposed.
- M-Layer: Defines the areas where metallization will be deposited for current injection and provides device numeration.
- RS-Layer: The backside of the wafer is also contacted to complete the PN-junction that allows for current injection.

Both the K- and K1-layers were etched employing a silicon nitride mask, which provided a safe option for a perpendicular and anisotropic etching and met the needs for high-temperature etching that InP derivatives require, but introduces certain complexity by adding further steps.

The final devices previously manufactured through this process showed partial success, with only the devices where the ridged waveguides (RWG) were pushed back from the facet offering measurable light output. Those devices without this so-called RWG pushback showed little to no lasing capabilities, presumably due to topography interference between the RWG and the facet, which reduced the homogeneity and smoothness of the facet.

3.3 Objectives

The objectives of this work are thus the following:

- Demonstration of functional laser diodes based on GaAs with etched facets. It is hoped to achieve at least several laser diodes that show lasing capabilities, even if their performance is limited.
- Simplification of the process. By reducing the use of silicon nitride hard masks for each etching step, it is expected to simplify the process while keeping the quality and precise patterning of the structures. Defects can be avoided by using only resist as mask instead of using resist to pattern a hard mask.
- Optimization of the etching recipes. The extensive recipe testing of varying variables (pressure, gas ratio, addition of nitrogen) and other chemistries (CH_4/Cl_2) will provide valuable insight.

3.4 Proposal

This work proposes a significantly simpler version of the presented process while maintaining the quality of the devices by taking advantage of the benefits that GaAs wafers offer.

Every step of the practical work will be covered and the results will be examined to understand how the process can be further optimized in the future. Regular microscope inspections will be carried out to monitor the progress.

The goal will thus be to fully realize lasing diode devices using AlGaAs waveguides while unravelling the critical points along the process and learn about the physical and chemical nature of the steps involved. Once completed, the devices will present the next structure:

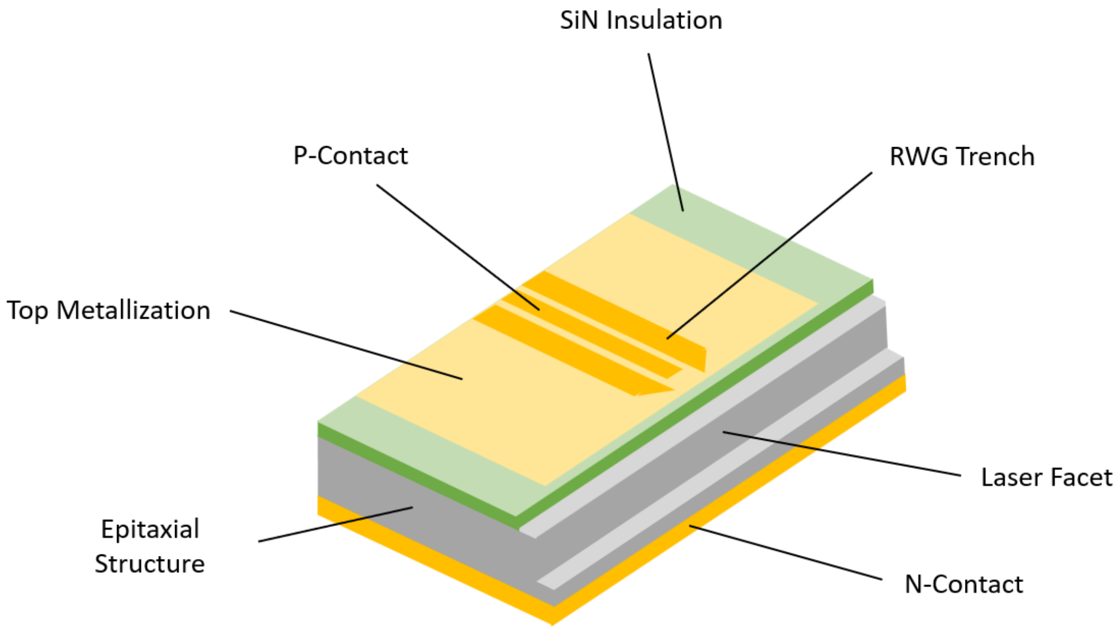

Figure 3.1. Schematic of the proposed laser diode structure indicating the elements of the device.

4 Front-end Processing

4.1 Process Overview

The front-end processing was split in two phases. Initially, two groups of test wafers were run in order to determine what kind of masking offered the best results and what variables had the biggest impact in facet quality. After these tests were carried out, a full process on epitaxial laser-structured wafers to manufacture the functional laser diodes was run.

For the initial tests, only a shortened version of the process consisting of the RWG and facet etching was used. Although the dummy wafers did not offer the possibility to perform measurements, they helped to determine the best recipes for facet etching and offer an introduction to the full device process, which is considerably more complex.

In the initial recipe testing, the two existing options for masking of the facet etching step (K1-layer) were considered: either only using a regular photoresist mask or employing a silicon nitride hard mask. Hard masks are most frequently used in etching processes that require high temperatures where the resist might burn. Even though this is not the case given that the etching processes can be performed at ambient temperature, its use can also offer higher pattern fidelity and more vertical profile angles. Therefore, this idea was tested.

However, the idea of using a hard mask for the ridge waveguide etching (K-layer) was discarded from the start in order to simplify the process, since silicon nitride hard masks require additional deposition and the RWG etch is not deep enough to take advantage of the benefits that they offer.

Consecutively, the full process of laser diode manufacturing was carried out on the laser epitaxial wafers making use of the best etching masking technique and recipes. Thanks to the addition of passivation and metallization steps afterwards, it was possible to measure and characterize the devices, comparing their performance and lasing capacities.

In total, 22 wafers have been used:

- 12 x GaAs wafers with a 3µm epitaxially-grown AlGaAs layer.
- 10 x GaAs wafers with epitaxy-grown laser stack layers.

4.2 Ridged Waveguide Etching

The first step that was performed to all wafers was the etching of ridge waveguides. As explained in the section about laser diodes, ridge waveguides are necessary for the optical confinement and guiding of light in the device. Although an appropriate aspect ratio and dimensions of the RWG have a positive effect on light guidance, verticality and smoothness are not as vital as with facets. Because of this, a simple well-tested recipe that had been previously used by the department was employed without further extensive testing:

BCl_3 (sccm)	Cl_2 (sccm)	He (sccm)	ICP Power (W)	CCP Power (W)	Pressure (Pa)	Temperature (°C)
50	5	10	300	100	0.5	30

Table 2. Recipe parameters used for standard RWG etching.

Previous to the etching, coating, lithography, and development steps were carried out. First, a cleaning and dehydration of the surface of the wafers were performed before coating and 0.7µm of positive resist. After that, lithography was performed on the stepper and the resist was then developed. An aluminum direct-contact carrier with backside He cooling was used for every etching step in this work, with the aim of keeping the temperature of the wafer as constant as possible. Finally, the wafers were inspected with the optical microscope to confirm correct patterning.

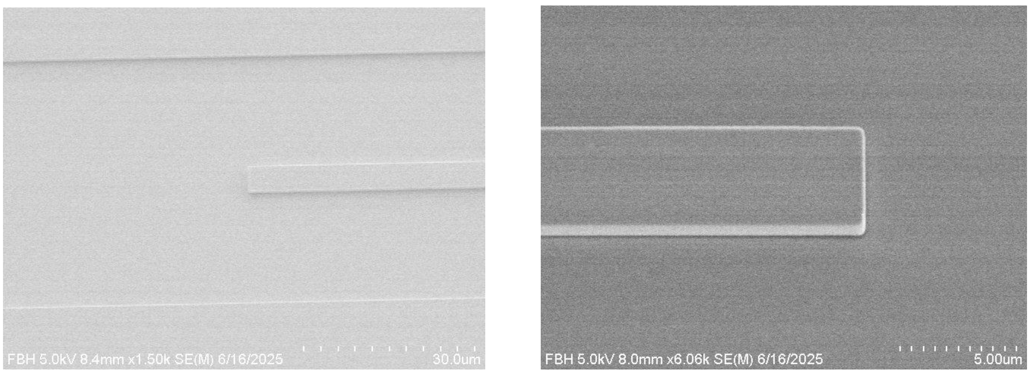

Figure 4.1. SEM inspections from wafer 5 and 6 after the ridged waveguide etching was performed.

The width of the RWG was 5µm and its thickness averaged around 1µm. The RWG pattern was precise and accurate. After the etching, the wafers were rinsed with water and dried by spinning to avoid chlorine cross-contamination. Additionally, both an O_2 plasma and lift-off process were tested to see which offered a better removal of resist. It was proven that lift-off was more efficient for resist removal and consequently the remaining wafers were therefore stripped in this manner.

4.3 Facet Etch with Photoresist

After the completion of the K-Layer, the K1-Layer processing was carried out. As previously explained, facet etching using photoresist and hard masks were tested in order to compare the quality of the etching process. The first batch of six wafers used a resist mask, while the second one received the silicon nitride deposition and necessary patterning.

The step consisted of a second lithography process, with its respective coating, exposure, development, and visual inspection steps. Next, based on past experience and the literature [22] [23] [30], a design of experiment was conceived focusing on the variables that would potentially have the biggest influence in roughness and profile angle:

Recipe	BCl_3 (sccm)	CH_4 (sccm)	Cl_2 (sccm)	He (sccm)	N_2 (sccm)	Pressure (Pa)
1	55		5	10	0	0.5
2	50		10	10	0	0.5
3	45		15	10	0	0.5
4	40		20	10	0	0.5
5	55		5	10	0	1
6	50		10	10	0	1
7	45		15	10	0	1
8	40		20	10	0	1
9	55		5	10	3	0.5
10	50		10	10	3	0.5
11	45		15	10	3	0.5
12	40		20	10	3	0.5
13	55		5	10	3	1
14	50		10	10	3	1
15	45		15	10	3	1
16	40		20	10	3	1
17		1.5	5.5	40		0.5
18		2	5	40		0.5
19		3	4	40		0.5
20		4	3	40		0.5

21		1.5	5.5	40		1
22		2	5	40		1
23		3	4	40		1
24		4	3	40		1

Table 3. Recipe experiment table for facet etching on wafer quarters.

In table 3, an experiment with recipes based on BCl_3 (recipes 1-16) and CH_4 (recipes 17-24) was set up, with parameters such as their ratio over Cl_2, the value of pressure, or the addition of N_2 being tested. Other process parameters, such as temperature (set at 25°C), or generated ICP and RF power (set at 300W and 100W, respectively), were kept constant, since they were not expected to have great influence.

Four recipes could be tested in each wafer thanks to the use of a shadow mask, that is, a smaller silicon wafer laid on top of the actual one while etching which is cleaved in a way so that only a certain area is exposed. For this step, a shadow mask with a cleaved quarter through laser patterning was used. It was sequentially rotated 90° for each recipe to uncover another quarter and test another etching recipe.

A five-minute rinse was also applied to each wafer right after etching to stop possible chemical surface reactions on the resist mask after chlorine exposure. The photoresist that remained after the etching step was removed with the help of the lift-off equipment as previously decided.

Once the etching tests were completed, a SEM visual inspection as well as several measurements were carried out, such as the facet height, and the values of the measured variables, namely the etch rate and selectivity, were collected.

Next, the fifth and sixth wafers were processed employing the CH_4/Cl_2 gas mix. The results were disappointing, given the expectations of a faster etching. None of the mixes showed and etch rate higher than 150nm/min, which, when etched for the same period as the first batch of wafers, resulted in very shallow etching that did not serve for satisfactory facet formation.

Additionally, the formation of a crest-like structure could be observed in most areas around the edges where facet formation was taking place, which hindered precise profiler measurements and ruined the facets.

This undesired effect could be attributed to polymer redeposition, leading to local micro-masking in the area near these edges [24]. Given the high possibility of this effect happening in the facets of the laser diodes, the idea of employing a CH_4/Cl_2 mix for facet formation on the actual devices was rejected.

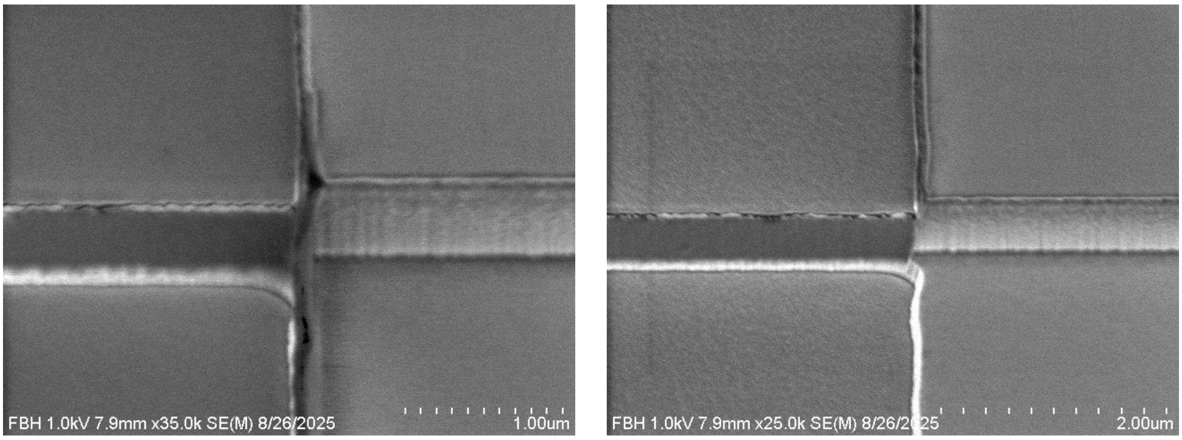

Figure 4.2. SEM inspection of facet detail from recipes 17 and 19. Redeposition-caused crest next to the facet to the left. Correctly facet etching to the right.

4.4 Facet Etching with Hard Mask

The next batch of six wafers were processed in exactly the same way to obtain the K-Layer. The same etching recipe based on BCl_3 and Cl_2 was employed and a visual inspection to confirm pattern accuracy was performed.

It was observed that RWG etching depth decreased to around 800µm with the same etching time and recipe, which could be attributed to different conditioning between the two days in which the process was carried out, but did not affect the results of the experiment given that we only want to replicate a similar topography and surface coverage as in the final devices.

After the K-Layer was completed, the first steps of the K-Layer were carried out. The deposition of the silicon nitride hard mask was performed through PECVD, resulting in 200nm of Si_3N_4 with a deposition rate of 0.763 nm/s and a refractive index of 1.994. The process made use of NH_3 as precursor to obtain Si_3N_4.

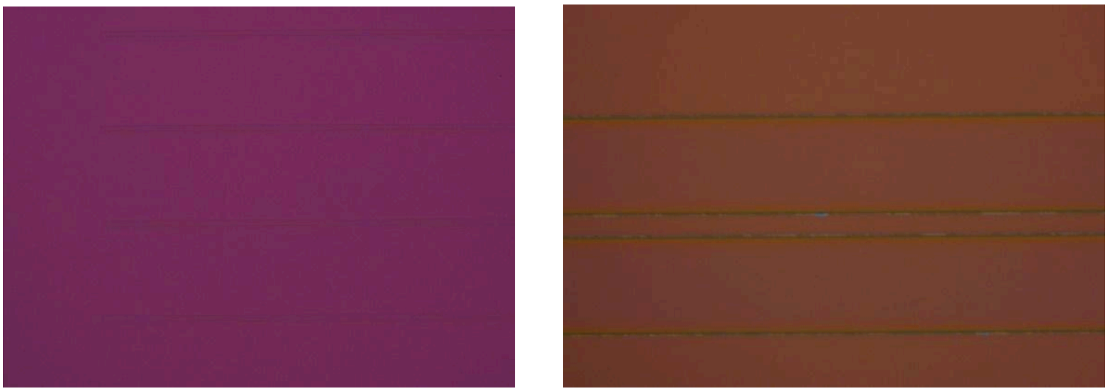

Figure 4.3. Optical microscope inspections of the RWGs of wafer 11 at 5x and 100x from wafer 10 after CVD was performed.

Afterwards, another round of lithography was performed, patterning the areas where the facets would be formed, following the recipes on Table 4. In the following images, the silicon nitride exposed areas (in purple) can be observed:

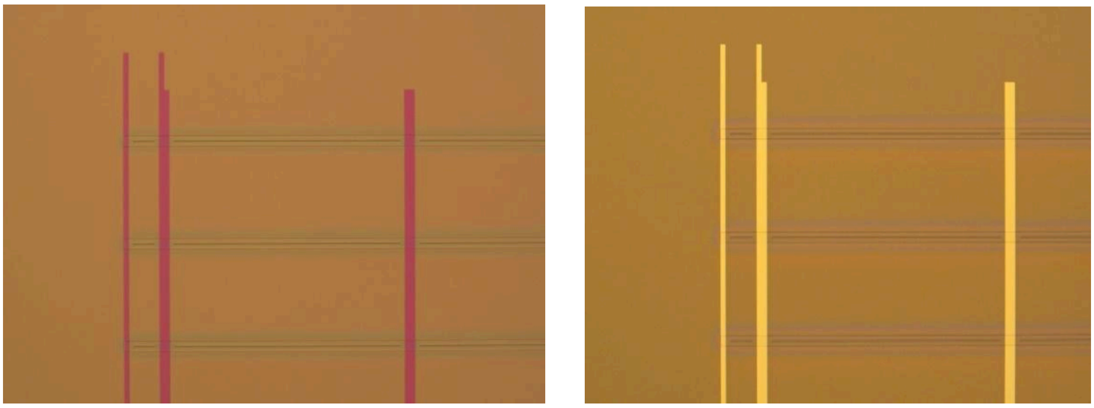

Figure 4.4. Optical microscope inspections at 5x from wafer 10 before, showing part of the Si_3N_4 CVD layer, and after the etching, with no traces of visible Si_3N_4.

The silicon nitride hard mask was opened with a CF_4-based recipe consisting of 10 sccm of CF4 with an ICP power of 100W and 1Pa of pressure. Both a previous and post O2 plasma etchings were performed to ensure no polymerization or byproduct redeposition took place, as well as a stripping of the resist. After the etching, no silicon nitride could be observed in the exposed areas.

Afterwards, the facet etching was carried out, making use of shadowing by quarters and monitoring the reflectivity change in three spectral wavelengths (488nm, 633nm, 950nm). Although the same design of experiment was used for these wafers, the etching times were lengthened to replicate the facet height and etching times that we would later need for the laser epitaxial wafers.

Etching times ranged from 14 minutes in the fastest case to more than 22 minutes in the slowest, showing a clear etch rate dependence on the recipe.

Unfortunately, the etch times were dragged too long with the intention of ensuring that the resist and silicon nitride layers would be completely removed. This led to unexpected overetching in the now exposed areas while the RWG trenches, which already had a thicker layer of resist on top due to topology-induced resist irregularities, remained covered, resulting in pattern inversion.

Even though the pattern inversion would render the actual laser devices useless, the height of the facets was still somewhat correct and the performed measurements, considering the remains of silicon nitride and in some cases resist on them, could still be of use and compared to the previous ones.

The etch rates, as it will be seen in the next section, were between 10% and 20% higher. This was due to the inclusion of the Si_3N_4 remains the measurement, corresponding to these percentages. Regardless of these variations, the etch rates and selectivities for each recipe showed consistency when used with a resist mask or a silicon nitride hard mask.

Regarding the visual inspection with scanning electron microscopy, it was be confirmed that the pattern of the ridge waveguide had been inverted. Additionally, due to the deterioration of the silicon nitride mask, a rounding of the edges was also noticed, which in our case presented an important problem. The use of two layers as a mask can pose difficulties if the transition between the two is not smooth and their verticality is not matched.

Once more, attempts with CH4/Cl2 were carried out. This time, due to time constraints and the poor previous results, only two recipes were chosen to process two full wafers. The chosen recipes were recipe 17 and 19 from Table 3, given their faster etch rate and no redeposition, respectively.

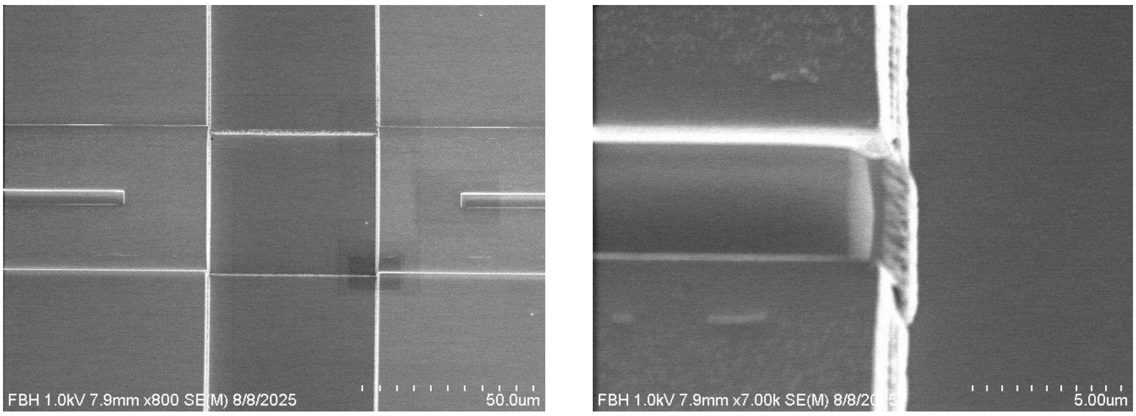

Figure 4.5. SEM inspections of wafer 7 after the K1 layer etch was performed. The RWG pattern was incorrectly etched into the wafer.

4.5 Results and Discussion

After carrying out these two variations of the process and assessing the quality of the results, the results provided by the two masking approaches helped determining whether it was advisable to etch the facets making use of a resist mask or implementing a silicon nitride hard mask based on the following results:

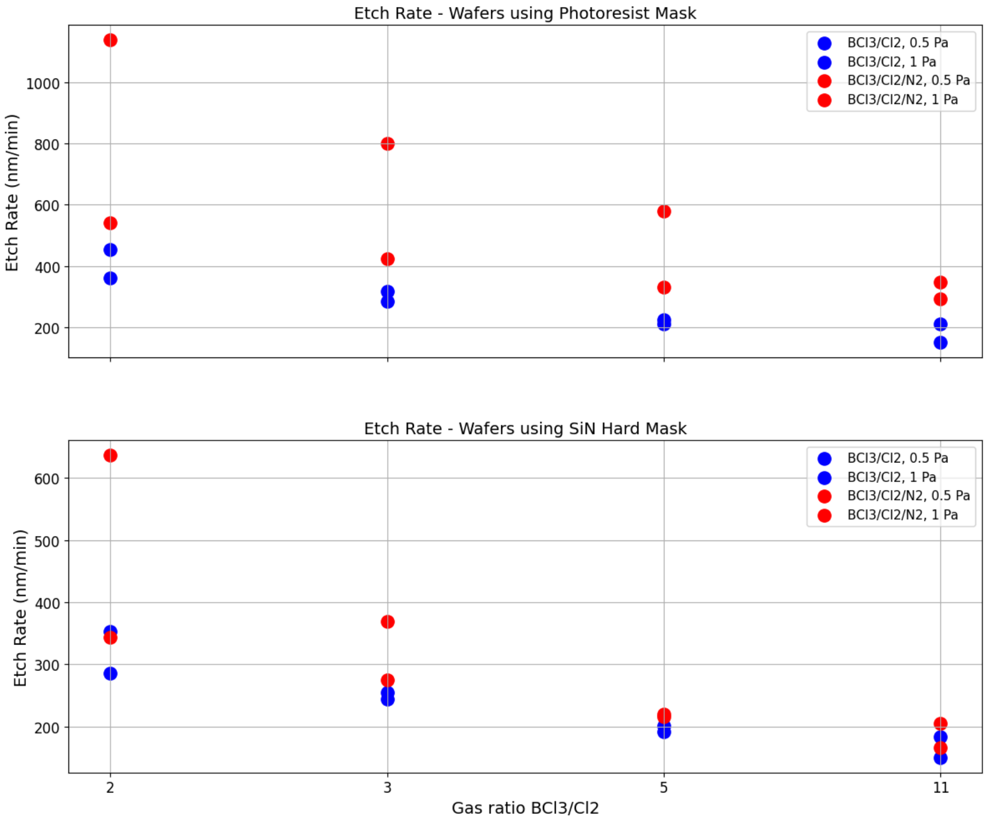

Figure 4.6. AlGaAs etch rate comparison obtained using a photoresist mask and hard mask.

Although the use of a silicon nitride mask usually helps to obtain vertical profile angles and improves selectivity in deep etching processes, it was shown that its inclusion in the flow added potential risks that, like in this case, could severely deteriorate the final device. Additionally, its inclusion increased the complexity of the process, involving extra chemical vapor deposition and etching steps.

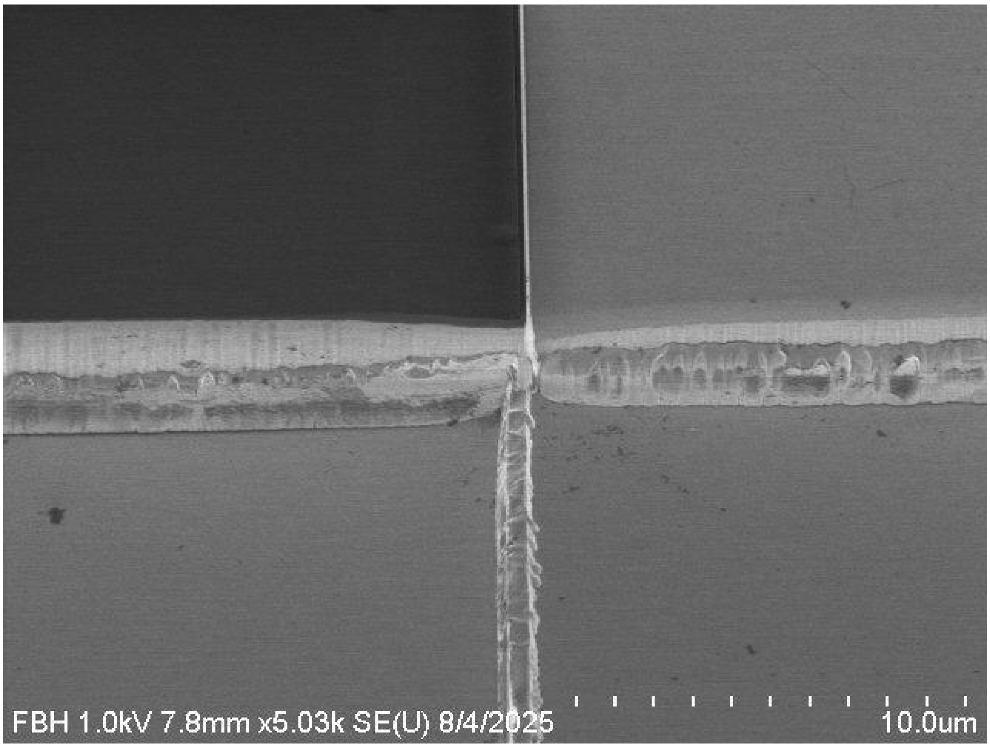

Figure 4.7. SEM inspection of wafer 7 showing poor facet formation when using a hard mask. The facet edge is in the vertical direction.

As it can be seen in figure 4.7, its usage did not offer any considerable improvements in obtaining vertical profile angles and the smoothness of the facet even worsened due to mask damage. Even if the cause lied on an incorrect deposition or etching, the higher probability of defects appearing was shown.

Taking into account these results, it was decided that the facets of the final laser devices would be etched with a photoresist mask, considerably simplifying the flow and providing vertical and smooth facets in pair with those already obtained.

The measurements taken after etching showed the following results:

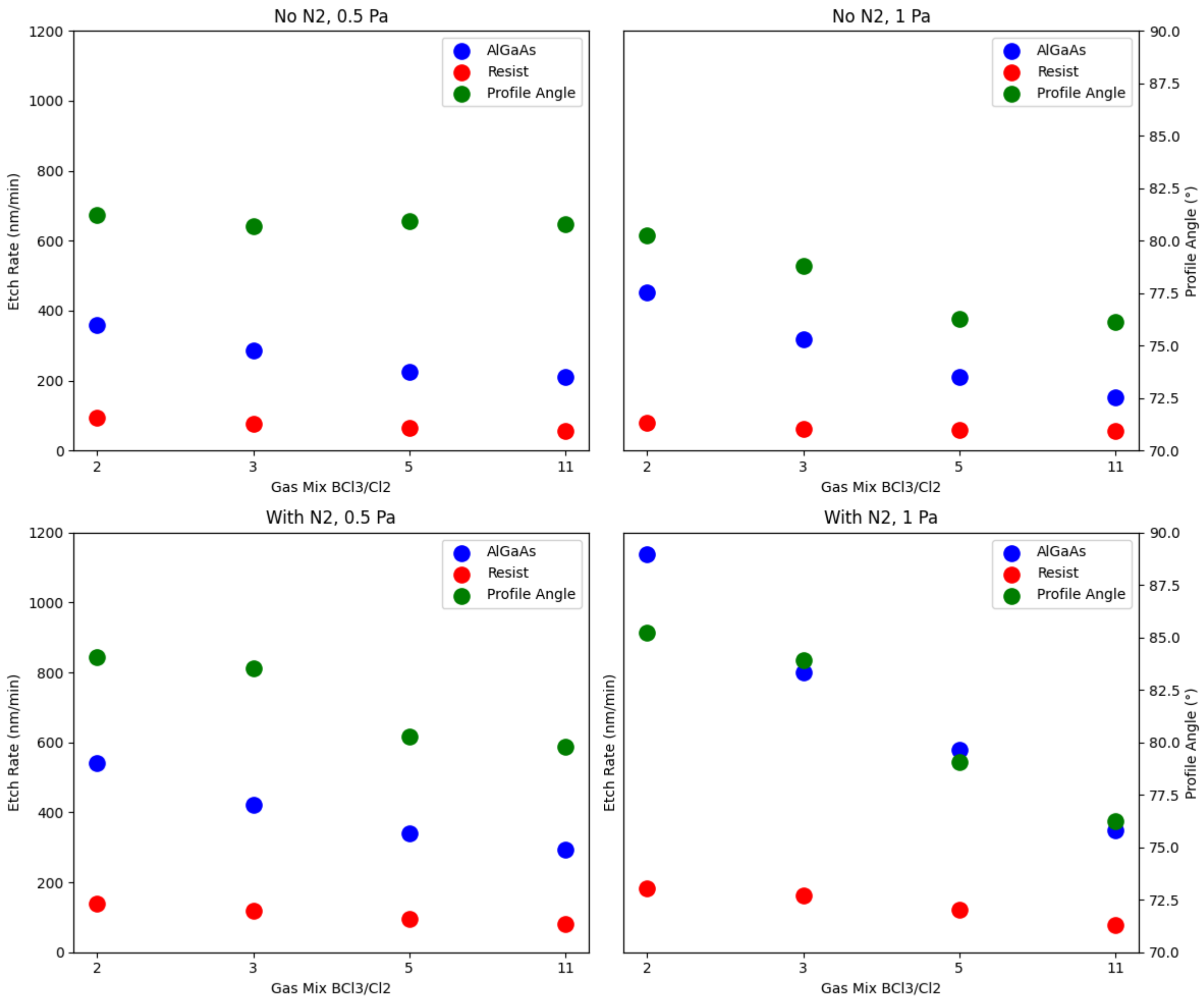

Figure 4.8. Etch rate and selectivity comparison between the recipes used with photoresist mask.

When it comes to pressure, it could be observed how recipes that used 1Pa of pressure offered slightly less vertical profile angles. As explained in the theoretical framework, this could be attributed to the higher chemical aspect of an etching at higher pressure, given the larger number of chemical reactions taking place in higher-density gases.

Concerning the inclusion of nitrogen in the gas mix, the verticality and smoothness of the facets were visibly increased without repercussions on any other variable, proving that it could be included in the recipes.

Finally, the examination of the ratio between the reacting gases, BCl_3 and Cl_2, shows interesting results. A seen in the graphs, lower ratios of BCl_3 over Cl_2 result in higher etch rates in all cases, which, although not crucial for the final results, is still beneficial for processing times.

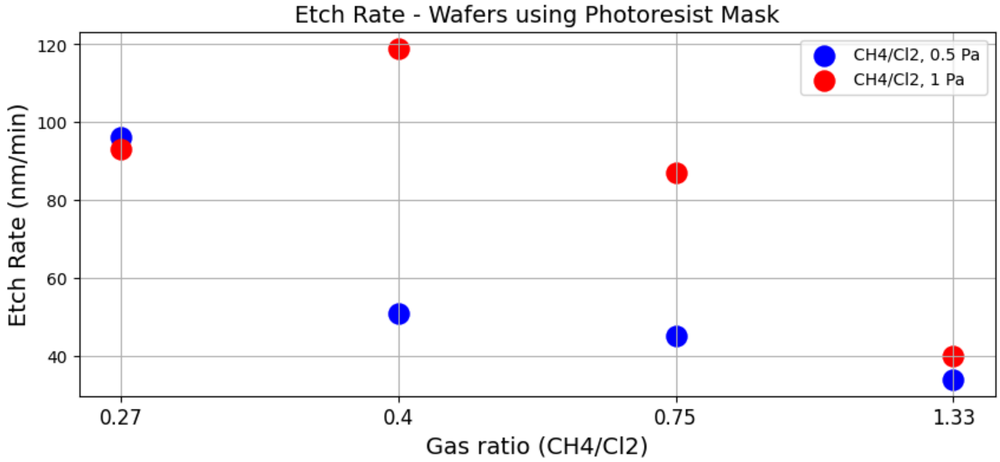

Figure 4.9. Etch rate comparison obtained with CH_4/Cl_2 gas mix at different pressures.

When it comes to the CH4/Cl2 mixes, given their considerably lower etch rates and facet quality were not ideal, it was decided not to carry out attempts with recipes containing this gas mix to avoid potential risks. In order to determine if the redeposition effect could be reduced with a longer etching or different epitaxy and acceptable results could be obtained, further tests can be carried out in the future.

After analyzing the data, the two recipes showing the best results were:

Recipe	BCl_3 (sccm)	Cl_2 (sccm)	He (sccm)	N_2 (sccm)	ICP (W)	RF (W)	Pressure (Pa)	Temp. (°C)
1	40	20	10	3	300	100	0.5	25
2	40	20	10	3	300	100	1	25

Table 4. Best recipes from the tests and initial recipes for facet etching in laser epitaxial wafers.

4.6 Full Device Process

After the material for the laser diodes was ready and the recipes for the main steps were decided, the full device manufacturing process started.

Wafers 2 to 10 presented epitaxy layers consisting of: a top thin layer of GaAs that hinders AlGaAs oxidation (100nm), a p-doped AlGaAs top cladding (1090 nm, 25% of Al), a p-doped AlGaAs waveguide layer (800 nm, 15% of Al), the active region (101 nm), an n-doped AlGaAs waveguide layer (4000 nm, 15% of Al), and an n-doped AlGaAs bottom cladding (830 nm, 25% of Al).

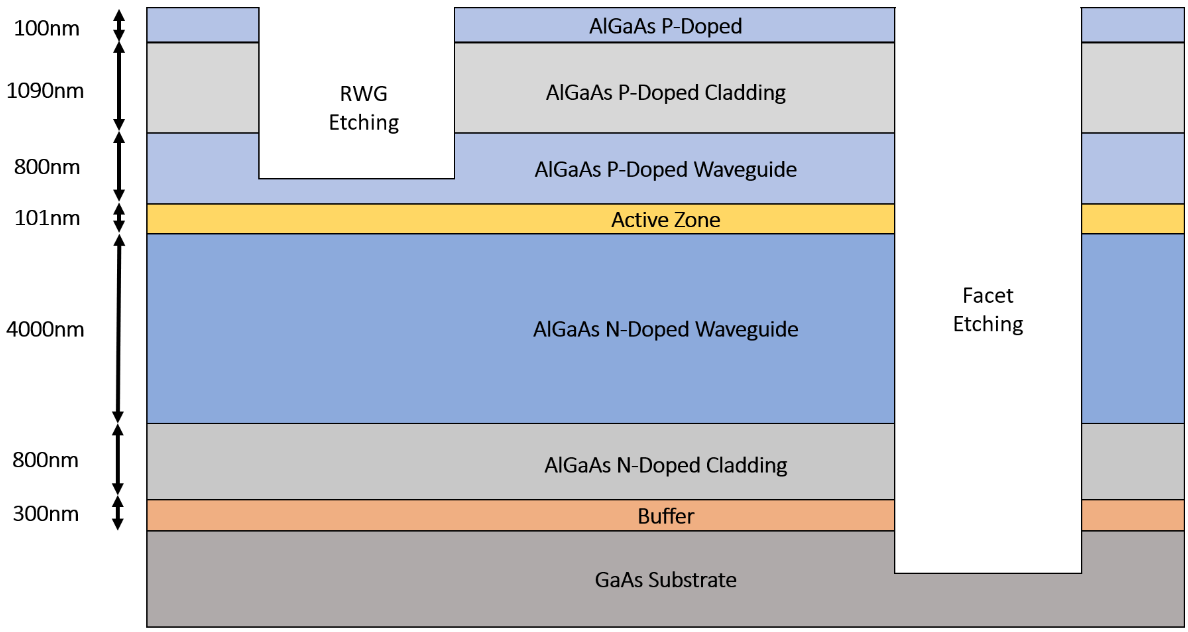

Figure 4.10. Schematic of the epitaxial structure of the wafers with the depth of the two etching steps.

Wafer 1 had a slightly different epitaxy compared to the other wafers, with a hardly thinner p-doped cladding and active area. Due to material availability, it was decided to still include it in the batch given that its epitaxial structure was very similar. The epitaxial structures were grown employing MOVPE on bulk GaAs substrate.

Additionally, a new approach for RWG design was taken. While the previous mask patterned rectangular RWG that ended several μm before the etched facet, a new reticle design with a RWG consisting of two lateral trenches with a triangular end was conceived by the optoelectronics department. The main advantage of the new reticle was the disappearing of the influence of topology on the facet etching process. By doing so, the influence of the topology of the RWG was minimized and undesired effects or defects were reduced.

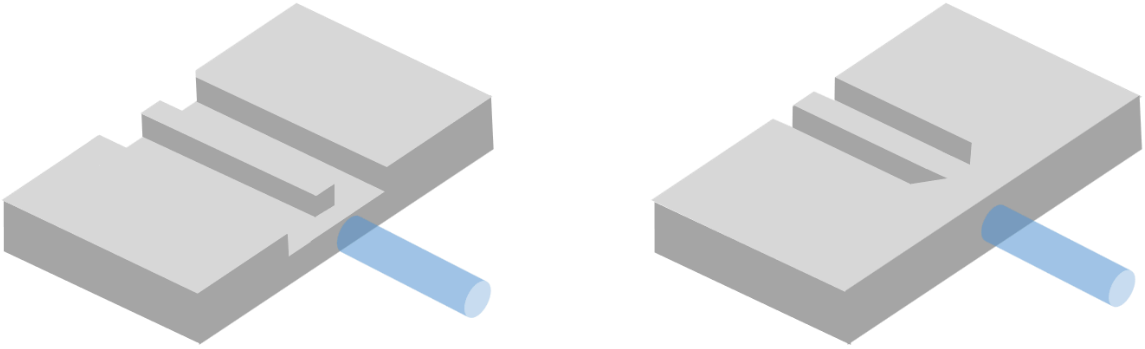

Figure 4.11. Old and new reticle approach for the RWG design, respectively.

The full process, which was conceived by the optoelectronics department for previous works, consisted then in the five layers introduced in section 3.1: K-Layer, K1-Layer, I-Layer, M-layer, and RS-Layer. In this case, in contrast to the regular flow, it was decided to move the K1-Layer after the I- and M-Layers to delay the facet etching as much as possible and avoid contamination until the end.

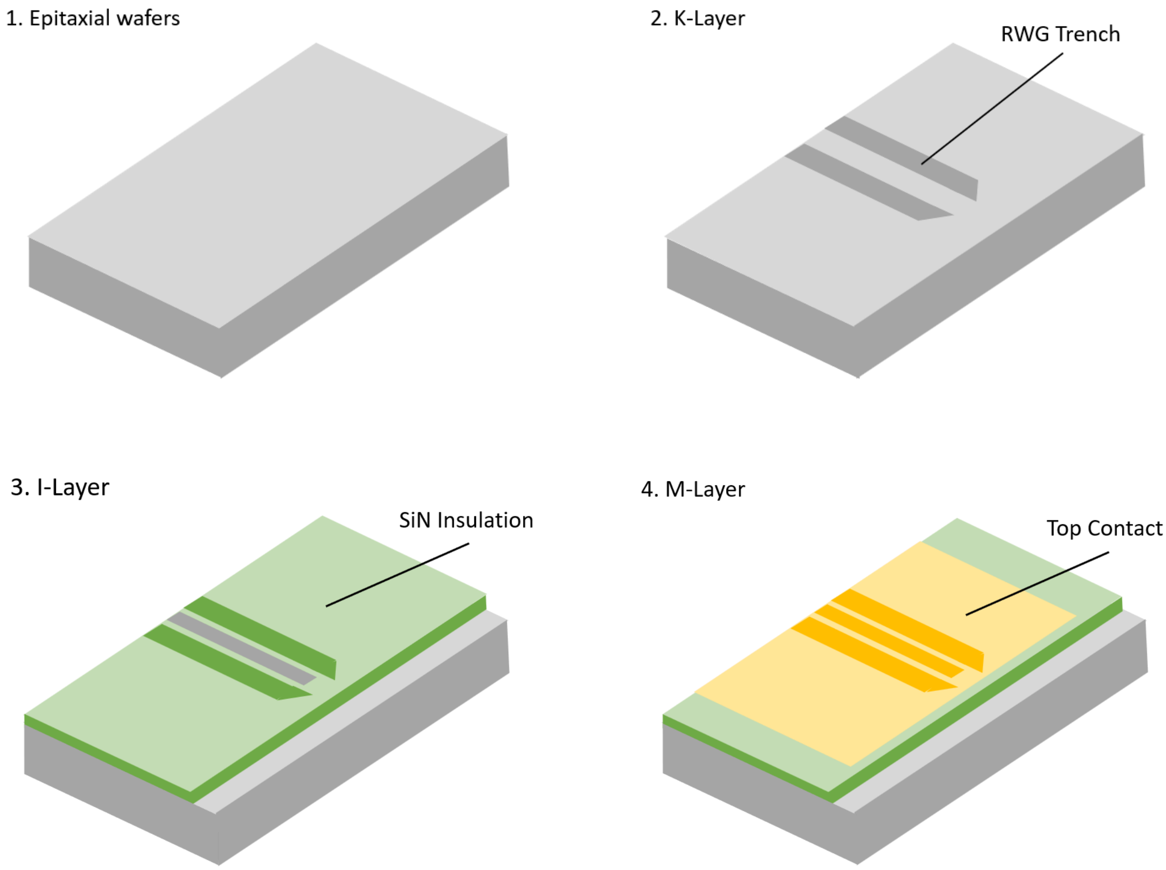

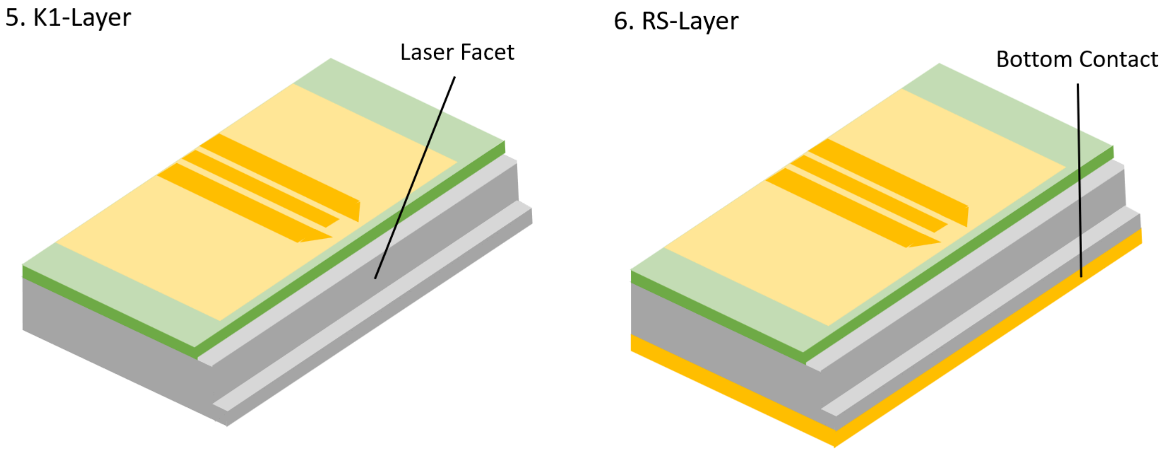

Figure 4.12. Visual flow of the 6-layer full device process for the diode lasers.

4.6.1 K-Layer

The K-Layer consists of the ridge waveguides that confines and guides the light through the device. Using lithography and a photoresist mask, the RWG trenches were patterned. A depth of 1.5µm was considered enough for light to be guided and the period simulations for the etch were carried out at 488nm, 633nm, and 950nm.

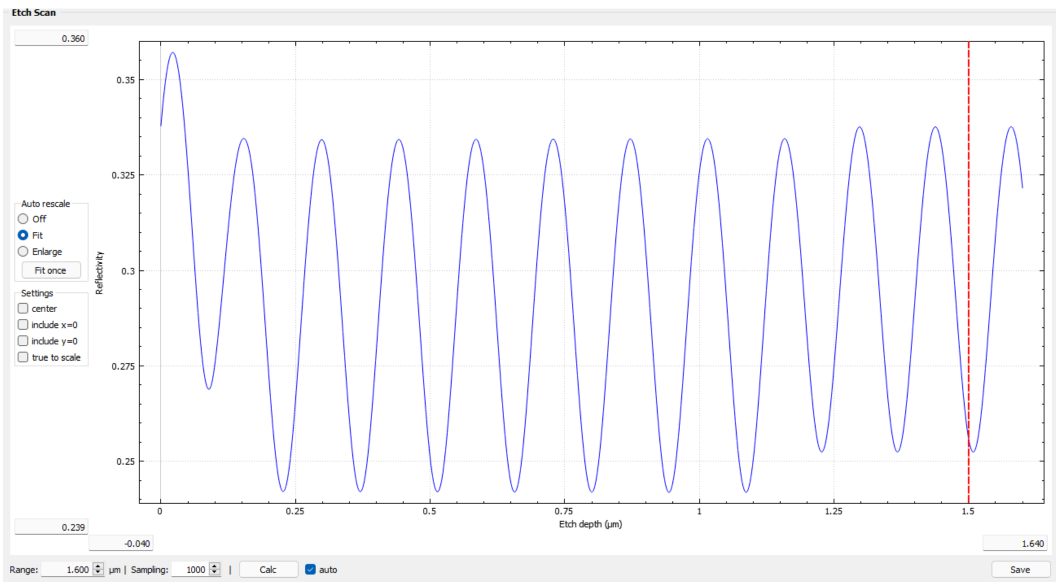

Figure 4.13. Reflectivity period simulation for a 1.5µm etch in a 950nm wavelength.

For the lithography steps, a positive SPR 955 CM 1.1 photoresist was used and an exposure of 100mJ/m^2 was selected. The recipe used for the etch was the same as in the dummy wafers, consisting of a mix of BCl_3, Cl_2, and He. After etching for 10.6 cycles and achieving a desired depth of around 1.5µm, lift-off was carried out along with visual inspection of the trenches and a measurement of the RWG height with the profilometer. All RWGs in the first batch were correctly etched with a precision of 0.5%. In the second batch, this precision was improved up to less than 0.1%.

1st Batch Wafers	1	2	3	4	5	6
Depth (µm)	1.494	1.522	1.484	1.483	1.499	1.547

2nd Batch Wafers	7	8	9	10
Depth (µm)	1.503	1.499	1.495	1.508

Table 5. RWG height measured in laser epitaxial wafers.

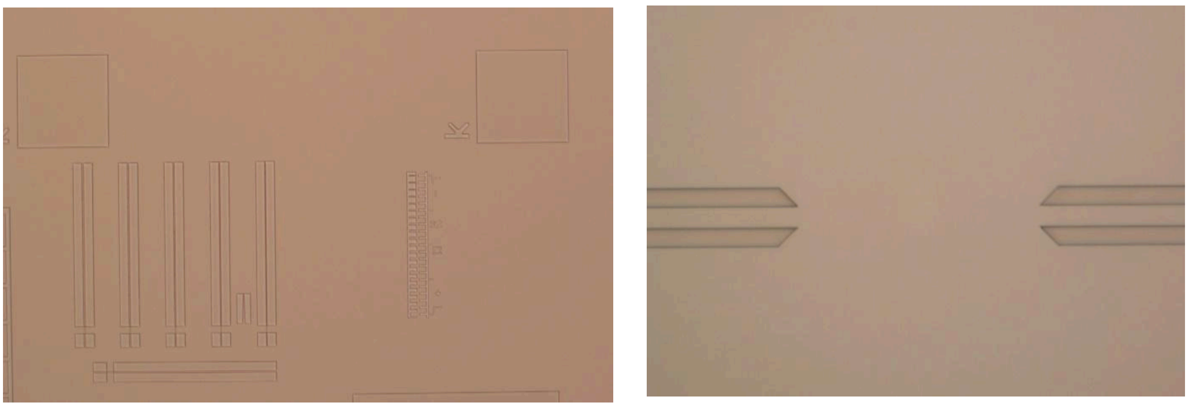

Figure 4.14. K-Layer details of wafer 4 inspected in an optical microscope. To the left, control structures of the layer. To the right, zoomed-in view of the new RWG design.

As previously explained, the shape of the trenches was different to those patterned in the dummy wafers after using the new reticle, reducing the influence of surrounding topology on the facet. The new design ensured that the area next to the facets was regular and both roughness and profile angles would not be put at risk.

4.6.2 I-Layer

For the insulation layer, the wafers were covered with a 100nm (wafers 1 to 6) and 300nm (wafers 7 to 10) of Si_3N_4. After carrying out the lithography process with positive AZ1518 photoresist, the exposed silicon nitride was etched away with an SF_6 plasma, leaving openings for the facet area and the top contact. Additionally, the wafer numbers for later device identification were also patterned, as it can be observed in figure 4.16.

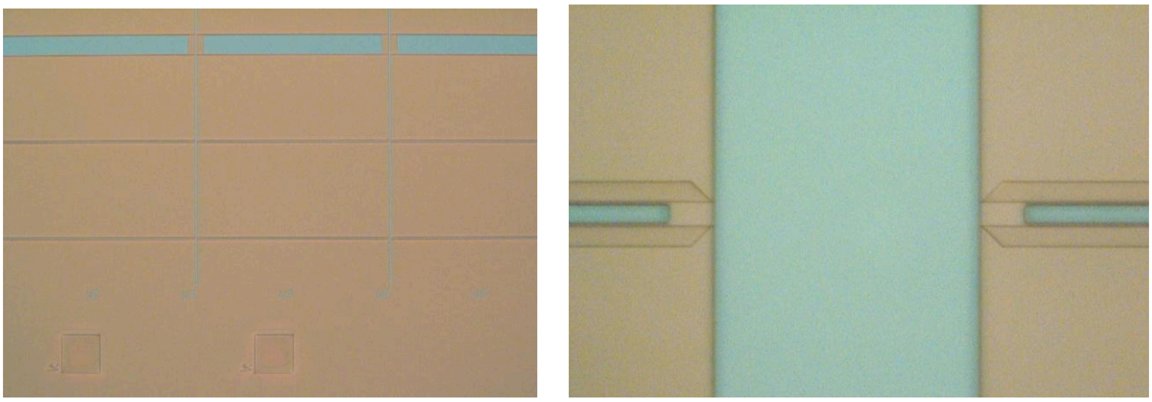

Figure 4.15. I-Layer details of wafer 1 inspected in an optical microscope before the etch. To the left, wide 5x overview of lasing devices and wafer numbering. To the right, 100x detailed view of facets.

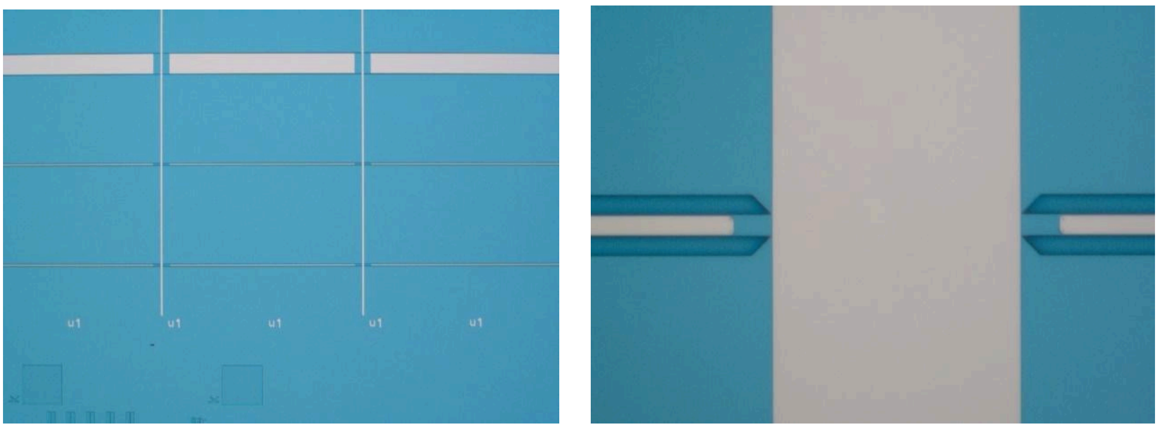

Figure 4.16. I-Layer details of wafer 1 inspected in an optical microscope after the etch. To the left, wide 5x overview of lasing devices and wafer numbering. To the right, 100x detailed view of facets.

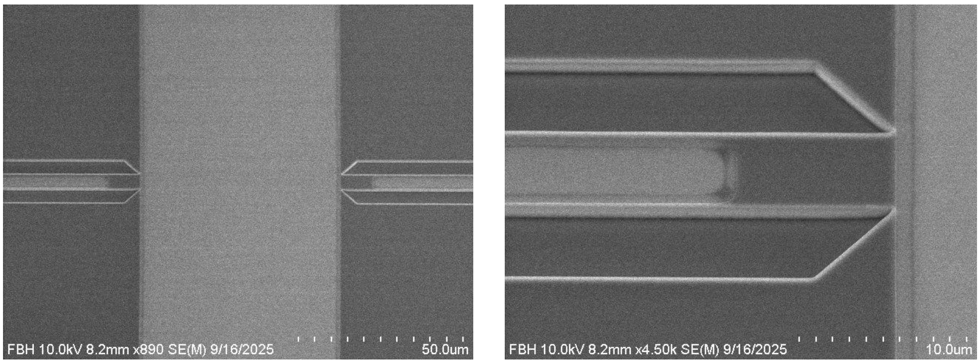

Figure 4.17. I-Layer details of wafer 1 inspected in SEM after the etching, showing surface coverage except for contacts and facet openings.

4.6.3 M-Layer

The metallization layer contains the upper metal contacts that allow for current injection into the device. The contacts consisted of a triple metal layer of titanium (30nm), platinum (40nm), and gold (575nm), which served as adhesive, solder barrier, and contact, respectively. This three-layer approach offered mechanical stability and optimal conduction. [31]

First, a lithography process with a negative resist was performed. Then, the three layers of metals were deposited on top of the resist. Finally, a lift-off step was carried out, exposing the areas where resist was present and leaving the devices covered with metal expect for the facet and cleaving areas.

After these steps were completed, the contacts were formed in the areas where the metals were directly touching the device, which corresponded to the areas where openings were left in the Si_3N_4 insulation layer. The reticle also contained the numeration of the devices for later wafer identification as well as their length.

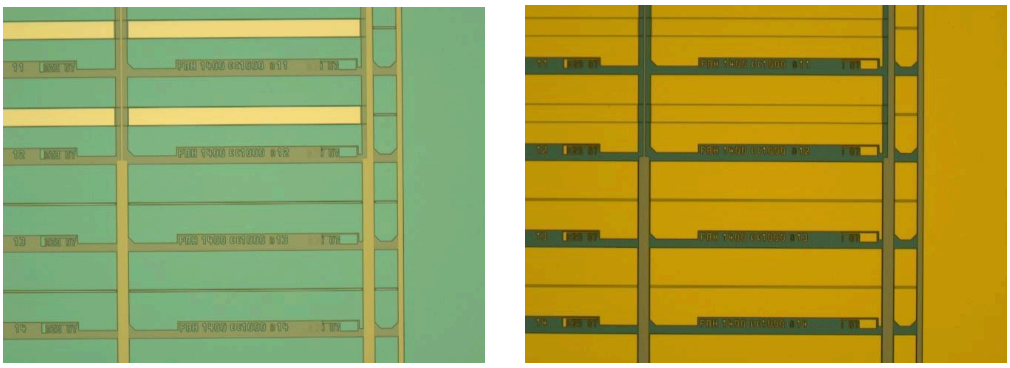

Figure 4.18. M-Layer optical inspection of wafer 1 showing the individual devices and their identification number before and after contact metal deposition.

4.6.4 K1-Layer

The facet etching for the K1 layer followed the same procedure as the K-layer. First, the lithography process where the facet patterning took place was performed. A considerably thicker positive resist of 6µm was used given the depth that had to be attained for the facet trench. Provided that the epitaxy structures of the wafers are approximately 7µm thick, it was required that the facet was higher than this thickness to replicate a regular facet cleaving.

With the aim of etching in a precise way and closely monitoring the process, the usual simulation of the periodical variation in reflectivity at different wavelengths was performed and compared to the reflectivity measurements taken in-situ by the etching equipment. In this case, it was only necessary to wait until we did not see any reflectivity variation, meaning only the bulk of the wafer was left.

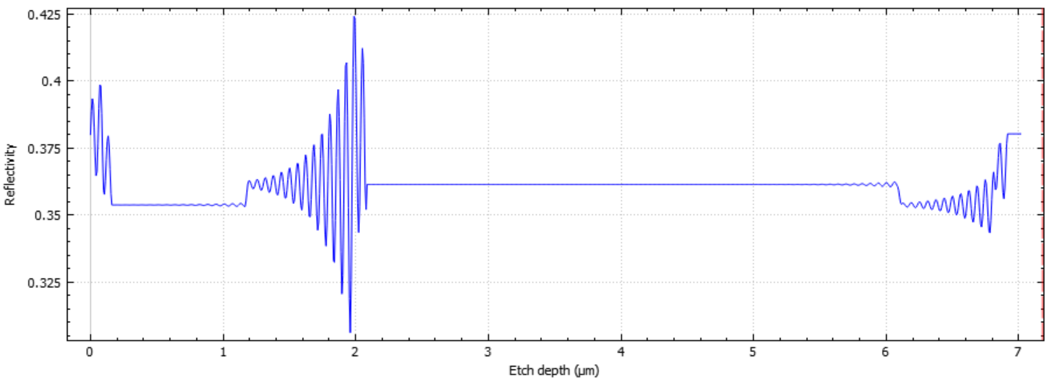

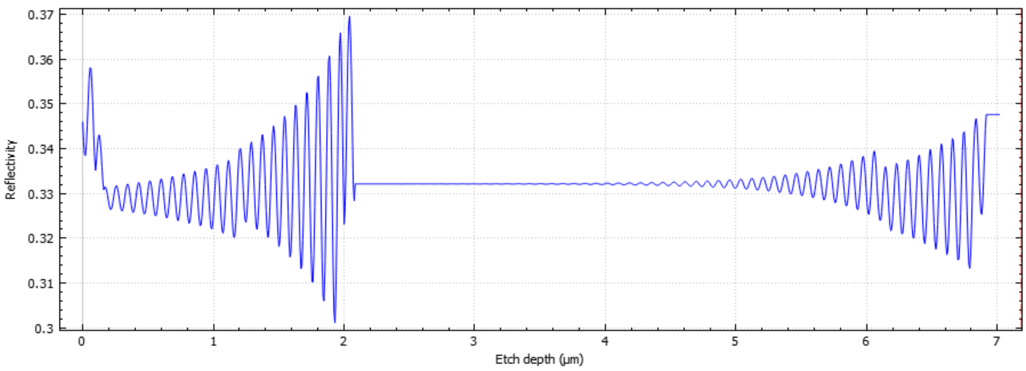

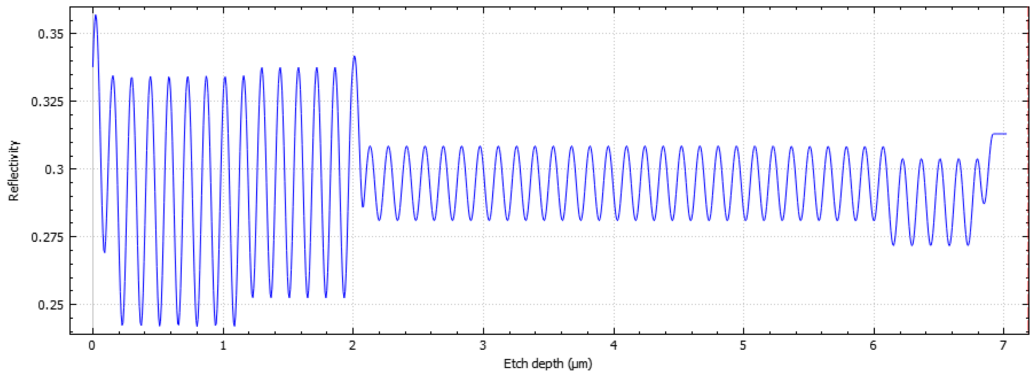

Figure 4.19. Reflectivity periods of the epitaxial structure at 488nm, 633nm, and 950nm, respectively.

The recipes used for facet etching in the laser epitaxial wafers followed thea new design of experiment:

Wafer	BCl_3 (sccm)	Cl_2 (sccm)	He (sccm)	N_2 (sccm)	ICP (W)	RF (W)	Pressure (Pa)	Temp. (°C)
1	40	20	10	3	300	100	0.5	25
2	40	20	10	3	300	100	1	25
3	30	30	10	3	300	100	0.5	25
4	40	20	10	3	300	100	0.38	25
5	30	30	10	3	300	100	0.38	25
6	40	20	10	5	300	100	0.5	25
7	25	35	10	3	300	100	0.5	25
8	20	40	10	3	300	100	0.5	25
9	20	10	10	3	300	100	0.25	25
10	15	15	10	3	300	100	0.25	25

Table 6. Recipes for facet etching in laser epitaxial wafers.

The first two recipes were determined by the results of the tests with the dummy wafers. Each following pair of recipes introduced variable modifications based on the results of the previous pair of recipes, aiming for improvement in each change. In the case of the recipes at 0.25 Pa, the total flow of the gases was reduced to half in order to allow for such low pressures, all while keeping the same ratios tested in their higher-pressure versions.

Figure 4.20. K1-Layer optical inspection of wafer 1 after lithography.

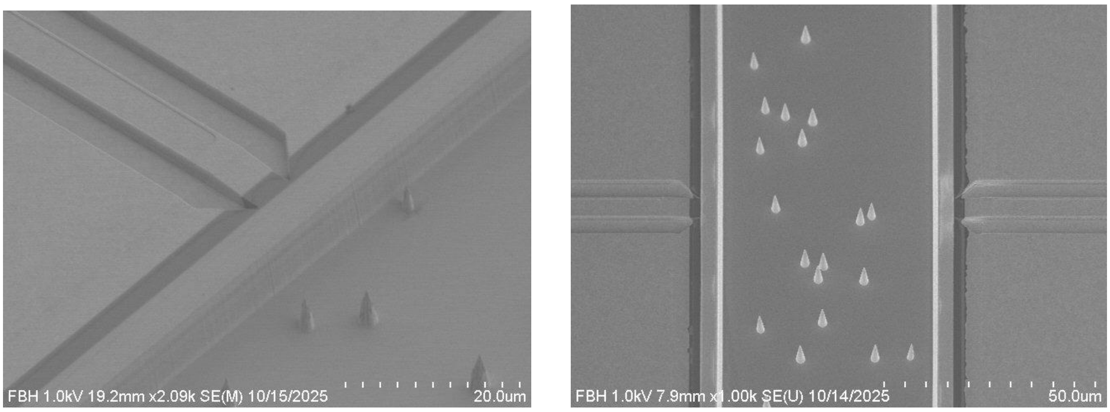

Figure 4.21. K1-Layer SEM inspection of wafer 1 after facet etching.

Above, pictures from the initial two wafers can be observed with their multiple layers, namely, the golden contact layer covering most of the surface, the end of the darker insulation Si_3N_4 layer, and the uncovered AlGaAs and GaAs trench.

It can be noticed that contamination micro-masking took place during this step. Some particles were present in the surface before the etching and their shape was amplified through this etching resulting in undesired cone-like structures at the bottom of the trench.

In order to reduce such contamination, an extra cleaning step right before the etching, consisting in a NH_4OH/H_2O bath, was implemented for the rest of the wafers. The results were very positive, with almost all undesired cone-like structures disappearing. Only very few still remained in the big test structure openings, but they did not interfere with the actual devices.

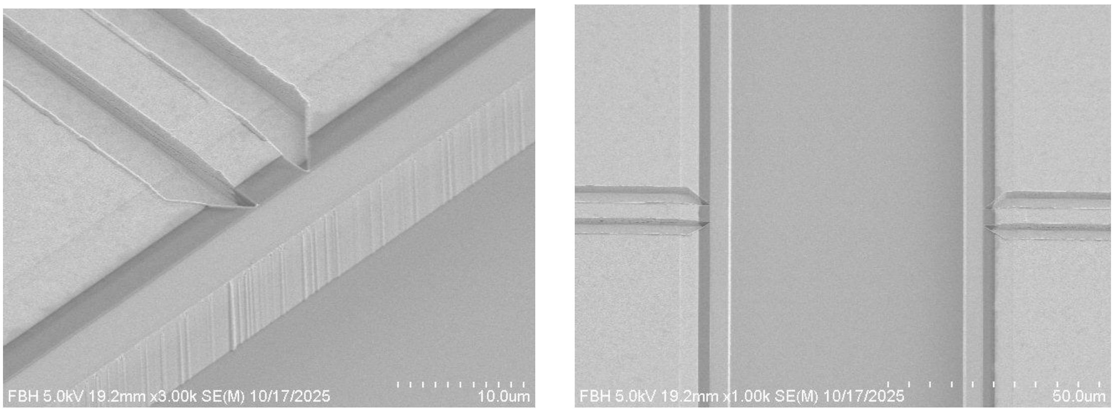

Figure 4.22. K1-Layer SEM inspection of wafer 5 after NH_4OH/H_2O cleaning and facet etching.

The devices could not be cleaved yet, given that the processing was still not complete. Therefore, in order to measure the profile angle of the facet walls, the following measurement method was conceived:

1. Facet height measurement with the profilometer.
2. Facet width measurement with SEM by taking a top view.
3. Calculation of the arctangent of the two values, which provides the profile angle.

This procedure was repeated for a facet in each quarter of the wafer and the profile angles were then averaged for each wafer.

The profile angle measurements were taken using this method because a profile shape direct inspection was not possible yet without cleaving the wafers. In order to confirm their accuracy, profile shape inspection on cleaved samples were taken after the device processing was completed. The results showed almost identical values to those previously measured.

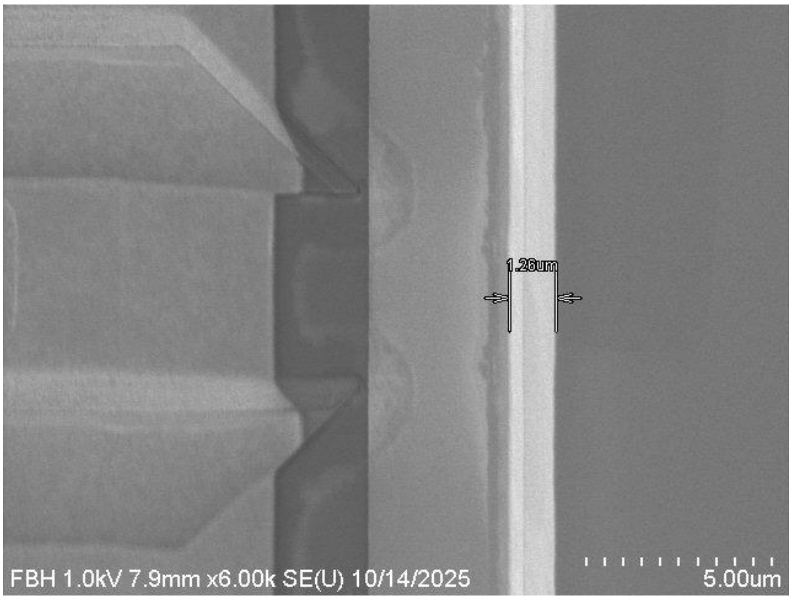

Figure 4.23. Measurement of a facet of wafer 2 width with SEM.

4.6.5 RS-Layer

Once the front side of the wafer was completed, a further processing of the backside (Rückseite in German, which gives its name to the layer) was required. Several cleaning and preparatory steps, such as O_2 ashing, sputtering of Ni and AuGe and rapid thermal annealing, were performed to produce ohmic n-contacts.

Similar to the p-contacts over the devices, the n-contact reinforcements on the backside of the wafer were also deposited, consisting of a similar Ti (30nm), Pt (150nm), and Au (300nm) structure. They were finally heated up to 250°C in the oven prior to the cleaving step, in which the wafers were cleaved into individual devices and ready for the final measurements. [32]

Taking a final look at the fully-processed wafers before cleaving, the golden color of the contact and the darker patterned section covered by Si_3N_4 can be observed:

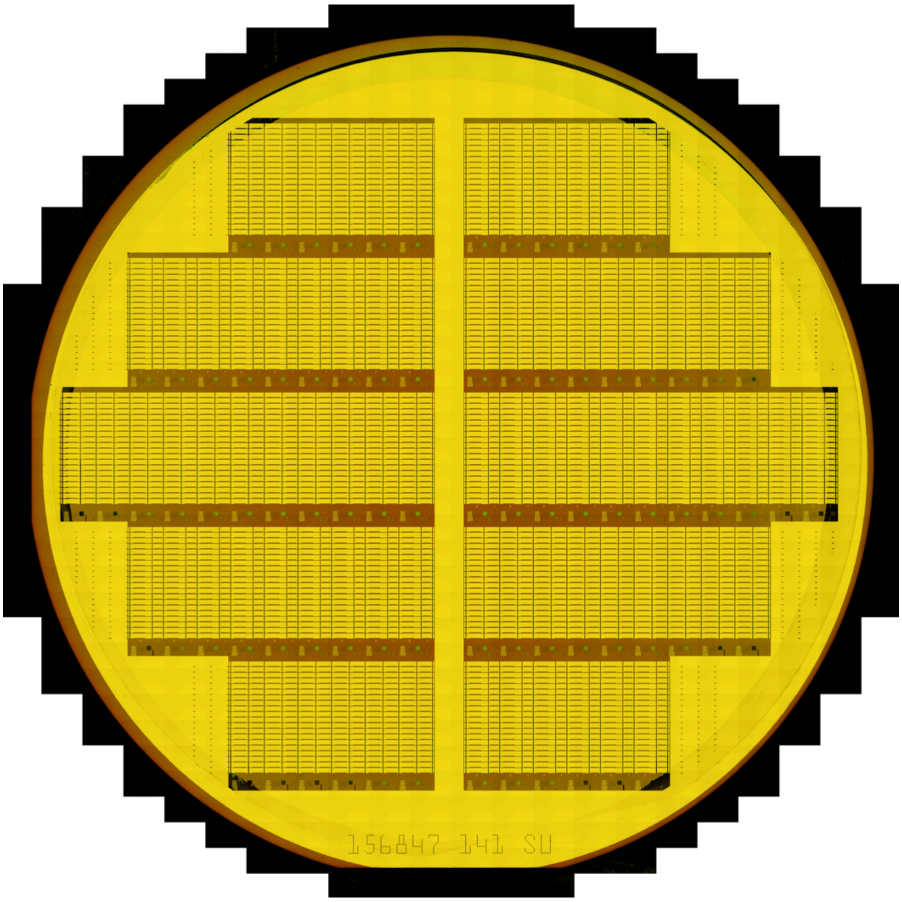

Figure 4.24. Top mapping of wafer 1 with the optical microscope before cleaving.

4.7 Evaluation and Characterization of Devices

Once the front-end processing was completed and the devices were cleaved in bars, multiple measurements were performed on the laser diodes: emission spectrum, power and voltage curves, and both vertical and lateral farfields.

The measurements were performed on a semi-automatic test station monitored by one technician at the institute. Each bar contained 20 devices, with different RWG widths (5µm or 100µm) and three facet configurations (cleaved-cleaved, cleaved-etched, and etched-etched). Laser devices also presented multiple lengths (1000µm, 1400µm, 1600µm or 2000µm), but due to time constraints, only the 2000µm LDs will be examined in the results discussion.

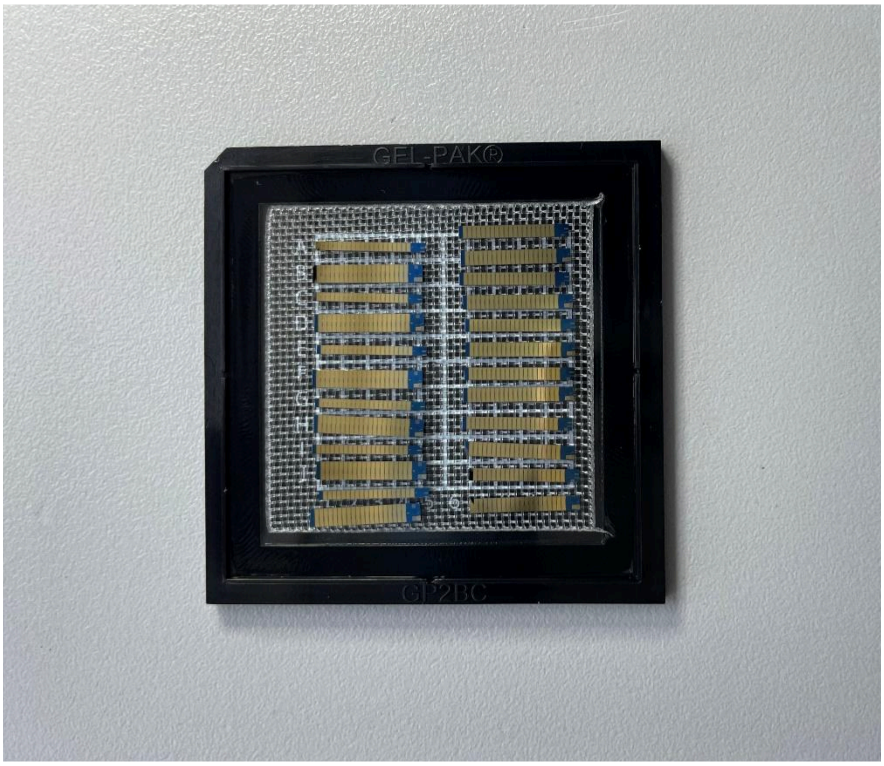

Figure 4.25. Top view of the cleaved devices after cleaving.

Once one bar was put into place, the four needles (first for power, second for voltage, and the rest for grounding to the metal holder) were laid onto the top contact of the devices, injecting the current that allowed for light emission. The needles sequentially moved from device to device to evaluate every diode.

Optical power was measured by two photodiodes via an integrating sphere. For the farfields, additional detectors were put into place. They sweeped the space in front of the facet describing vertical and horizontal arcs, determined by the angle limits defined by the user. In our case, the measurement was limited to 130° for vertical farfield and 70° for the lateral farfield due to the long measuring times required.

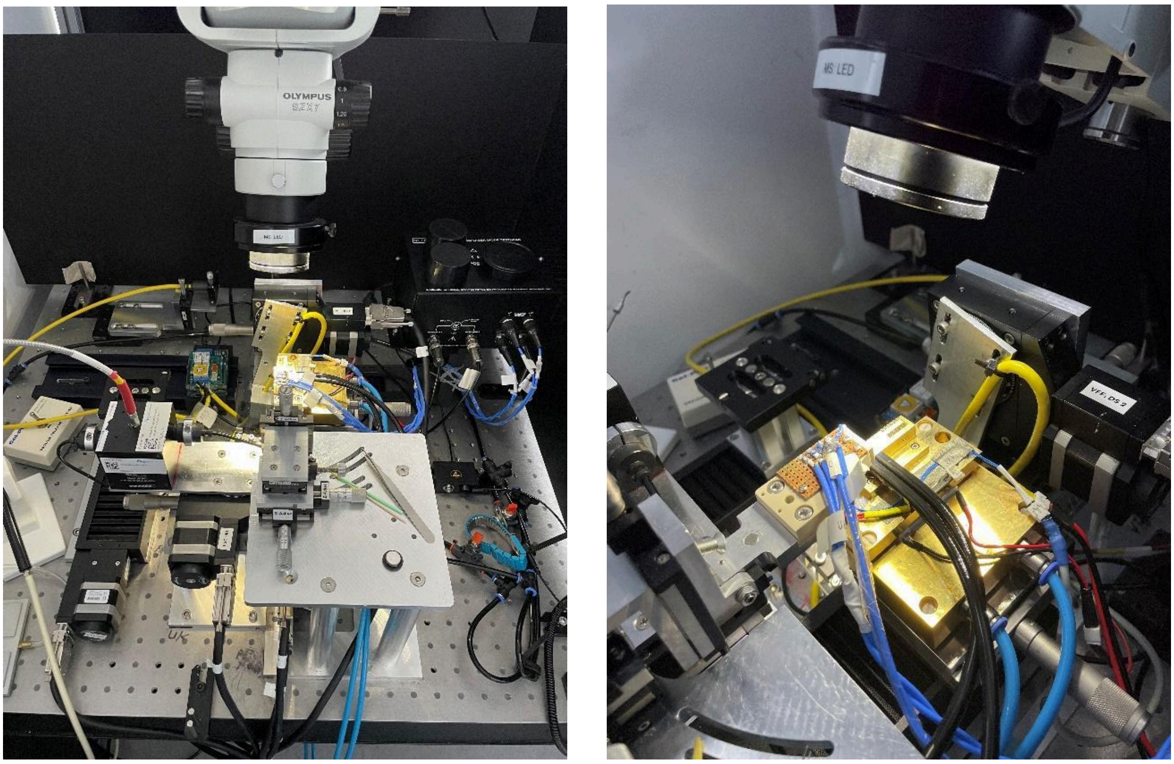

Figure 4.26. Measurement station where the results were obtained, showing the device holder, the top-view microscope, and the measurement devices.

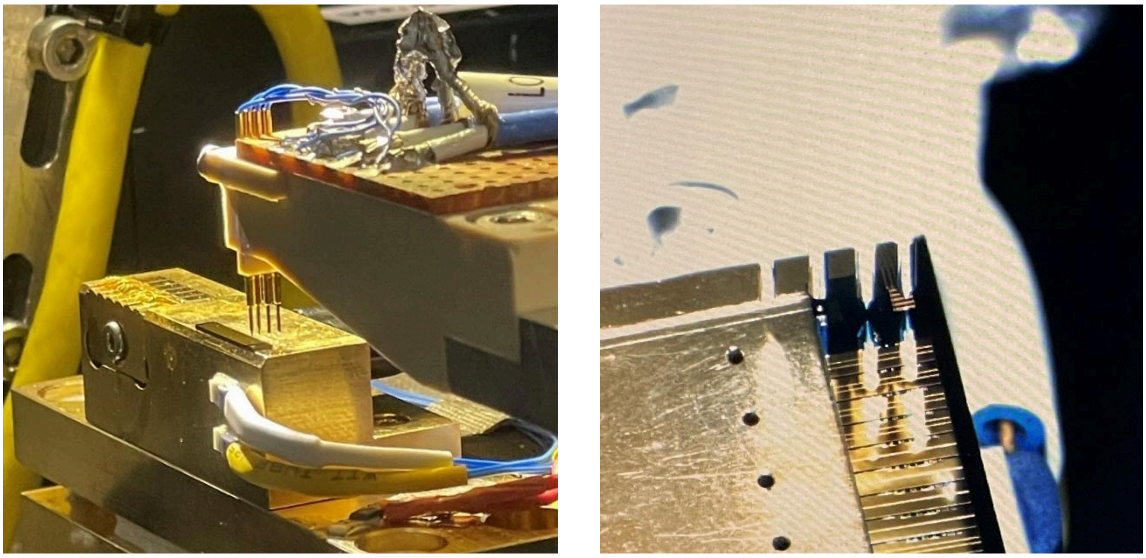

Figure 4.27. Detailed view of the device under testing before and during contact. Only two of the four needles are places on the device under test.

5 Results and Outlook

5.1 Results

5.1.1 Summary

Following the initial objective of creating functional laser diodes with etched facets on GaAs-based wafers, a simplified but efficient version of an already existing process was conceived and carried out. It consisted in the processing of 5 different layers, each one allowing for light guidance, insulation, light emission, and both p- and n-contact current pumping, respectively.

The main focus was placed on the facet etching step, which, as discussed, holds the most responsibility for the final performance of the devices, with recipe optimization both with previous tests on dummy wafers and with laser epitaxial wafers in order to understand the physical and chemical principles behind the process in a simplified case as well as its implementation in an actual application case.

Finally reaching the end of the practical work and diving into the results, it is time to discover whether the laser diodes showed functionality and, if so, what parameters presented the greatest impact on their light output quality. This will be done through a direct comparison taking cleaved facets as a reference to etched facets.

In the next two sections, the presentation of the results will be divided into an initial discussion of the insights that the recipe tests and experiments have provided and a following illustration of the multiple measurements performed on the final devices, putting them under several test conditions, and their results.

5.1.2 Recipe Optimization

As covered in the first sections of the practical work, initial recipe tests on dummy wafers were carried out based on recipes that worked in other studies as well as in the institute. These helped to obtain several recipes that already offered decent results and could be put into use with the laser epitaxial wafers. In that section, their results are examined in detail and the criteria for their selection is explained.

Right after that, the 10 laser epitaxial wafers were processed in smaller batches to further improve the recipes, with each result offering guidance on what direction to modify the parameters next. The profile angle achieved with these recipes are:

Wafer	1	2	3	4	5	6	7	8	9	10
Profile Angle (°)	81,1	81,9	86	85,4	86,2	83,8	84,1	85,4	85,6	85,5

Table 7. Average values of the achieved profile angles.

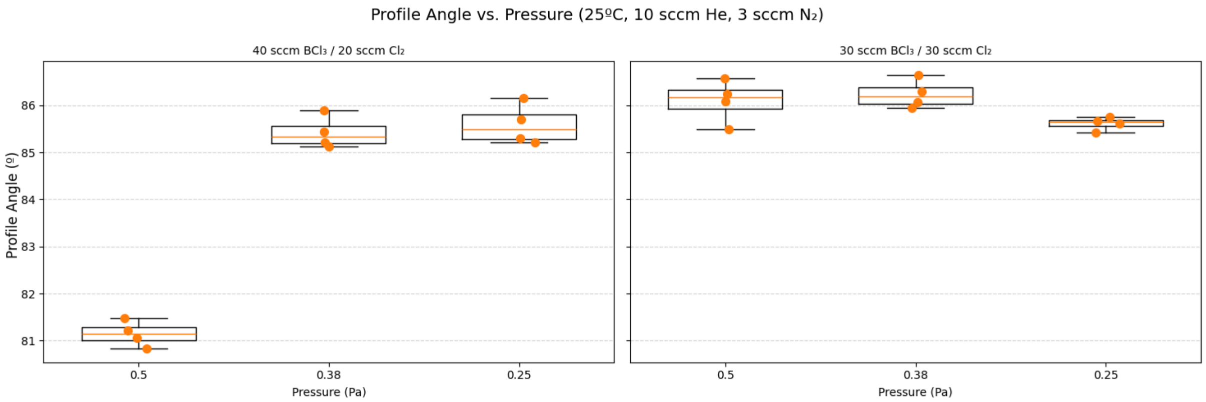

Figure 5.1. Influence of the pressure on the profile angle with different BCl_3/Cl_2 ratios.

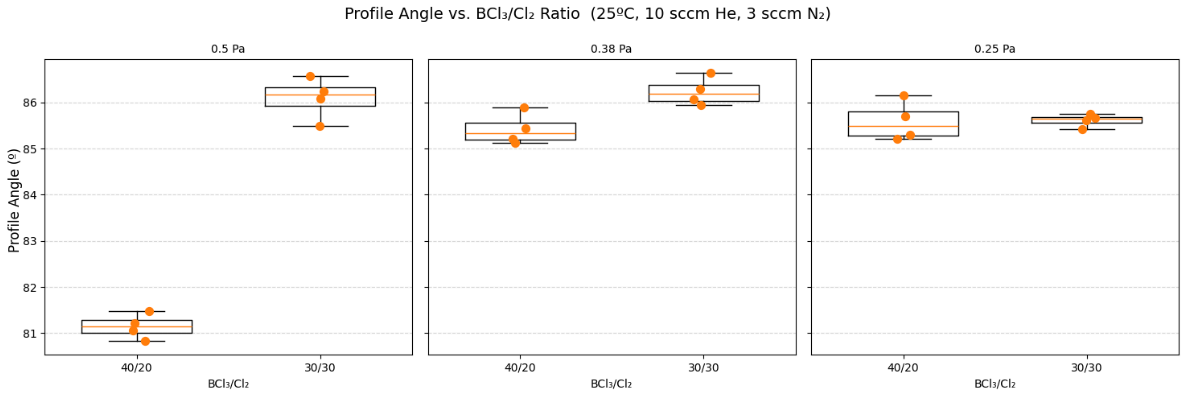

Figure 5.2 Influence of the BCl_3/Cl_2 ratio on the profile angle at different pressure values.

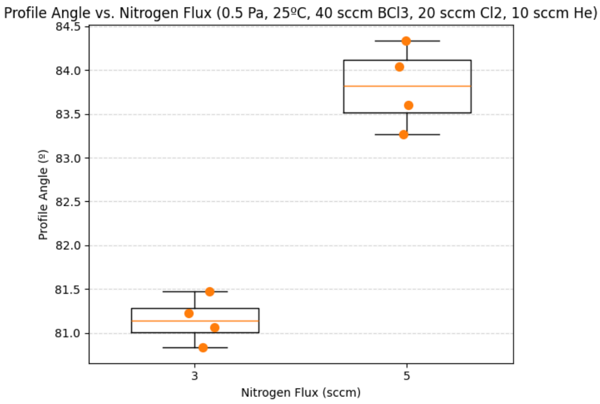

Figure 5.3. Influence of the N_2 flux on the profile angle.

Figures 5.1, 5.2, and 5.3 illustrate the dependencies of profile angle on the three main variables of the project: BCl_3/Cl_2 ratio, pressure, and the addition of N_2.

When it comes to the gas mix, a higher proportion of Cl_2 over BCl_3 in the mix appears to offer more vertical etching. Even though it could be assumed that a more notable presence of BCl3, which offers relative wall passivation, could lead to more vertical etching, the opposite is true given the higher concentration of Cl^- ion bombardment when Cl_2 is the main actor, offering faster etch rates and driving the etch deeper into the surface [33] [34].

The next step that helps improving verticality is the use of lower plasma pressures. This is due to the behavior of particles in a plasma. When a plasma contains more particles, these collide more often, diverting their trajectories and losing energy in the process. When the plasma presents a lower pressure and thus a smaller number of particles, these will impact into the surface more directly and with more energy [35].

Regarding the addition of N_2, in a similar way to BCl_3, N_2 offers side wall passivation which allows the etching to be driven downwards and not etch away in the horizontal direction. In the tests on dummy wafers, we already observed how the inclusion of a small amount of N_2 already improved the profile angle. Now, increasing the content of N_2 to even 5 sccm shows further improvement. However, this conclusion is based on one test and therefore more combinations with other further improvements should be put under test in order to prove if it is actually a general predictable trend.

The increase in etching anisotropy resulting in more vertical profile angles could very clearly be appreciated in those wafers with visible contamination masking, as the cone-like structures became closer to a vertical stick.

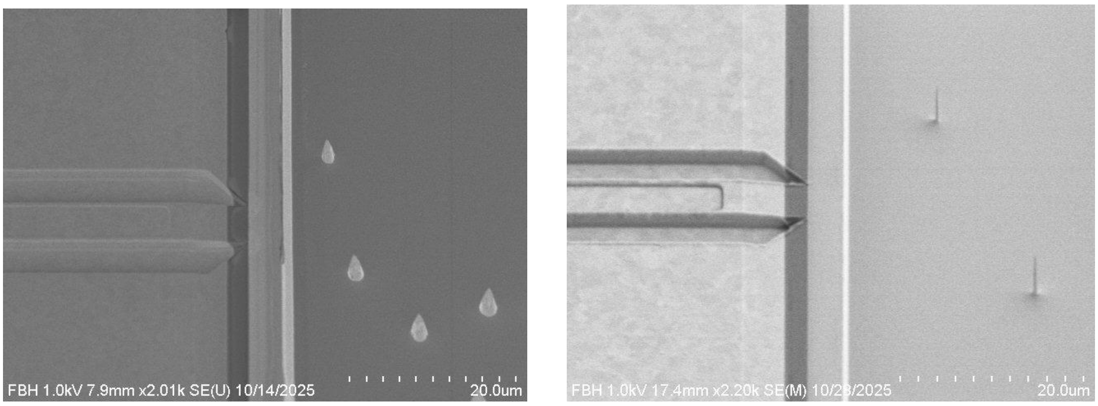

Figure 5.4. Vertical view of the undesired structures due to contamination masking. To the left, wafer 2. To the right, wafer 9.

Since the method for measuring the profile angles was limited, further confirmation of their validity was obtained cleaving the wafers after the electrical measurements were performed. The visual inspections and calculation of profile angles based on them confirm the previous results taken with a top view were correct.

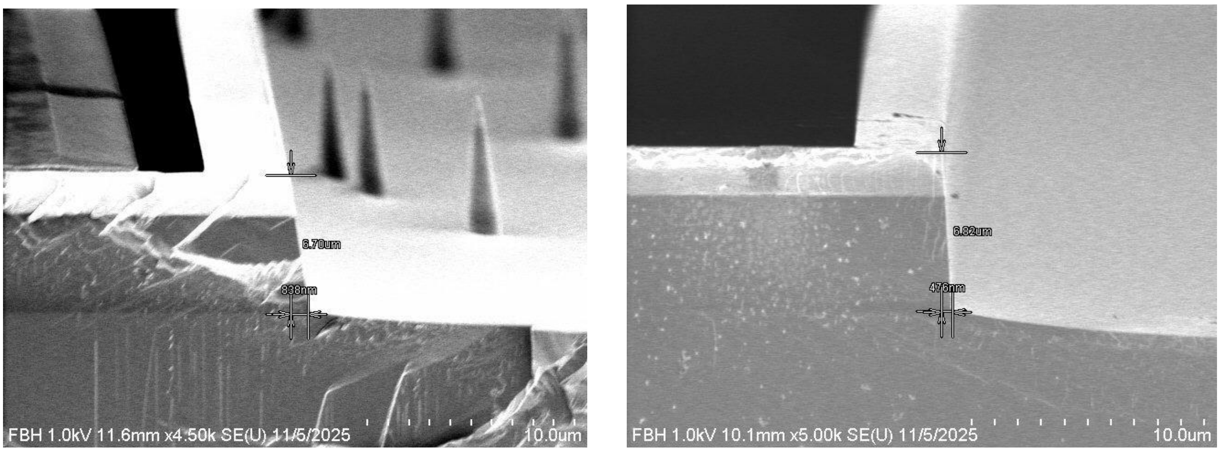

Figure 5.5. Measurements of profile angle after cleaving the devices. To the left, wafer 2. To the right, wafer 5.

These profile shape inspections after cleaving also confirmed the apparition of tailing. This behavior consists in a slightly deeper etch at the center of an exposed area that curves upwards until reaching the trench walls, in this case, the facets. Tailing can be caused by multiple reasons, such as an irregular distribution of radicals and ions or the redeposition of previously etched material [36] [37]. Even though fully flat facet trench bottoms are not required to achieve functionality in the LDs in our case (only etching deeper than the epitaxial layer is necessary), a more precise control and mitigation of this phenomenon would be of use for future optimization of the devices.

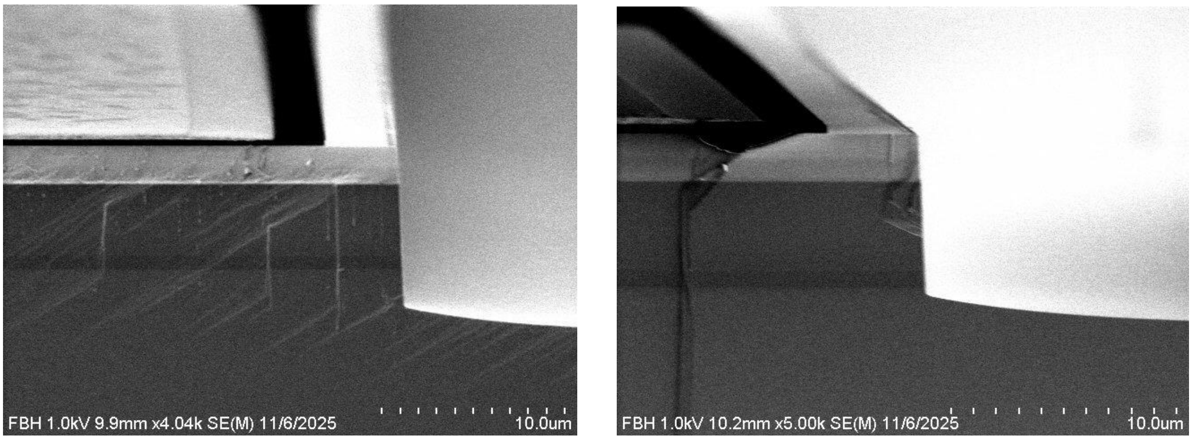

Figure 5.6. Undesired tailing taking place at the bottom of the facet trench. To the left, wafer 8. To the right, wafer 10.

5.1.3 Laser Performance

As explained in section 4.7, the evaluation of the lasers included multiple tests that assessed the spectrum width, the power and current curves of the devices, and both their vertical and lateral farfields. The results of these measurements will be presented hereinafter.

Given the wide range of devices present in the wafers, which present different lengths and RWG widths, the devices with comparable features and best results will be the focus of the results presentation. Only the devices with a length of 2000µm will be discussed. The devices will be addressed by the number of the wafer that they belonged to (1 – 10), with diodes from each wafer presenting different facet characteristics due to the recipe used for the facet etching, and by their RWG widths, either 5µm (narrow) or 100µm (wide).

Additionally, the laser bars contained laser diodes with three facet configurations: cleaved facets on both sides, etched facets on both sides, or one of each type. The cleaved-cleaved configuration will serve as reference for comparison. Devices emitted light on both the front and back facet, but only the measurements on the front facet emitted beams were considered in this work.

The first measurement that was performed was the spectrum of light emission of the devices, provided that the calibration for other measurements were based on this. The spectrum of the devices emitted through the front facet were:

Wafer 1

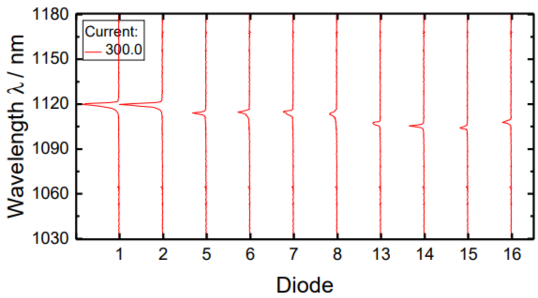

Wafer 2

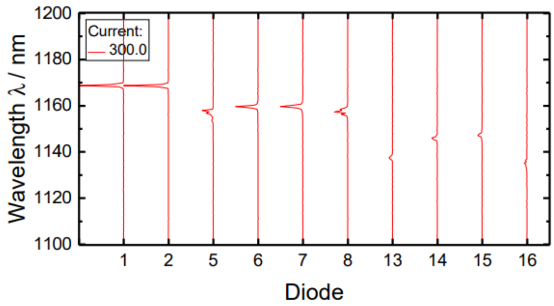

Wafer 3

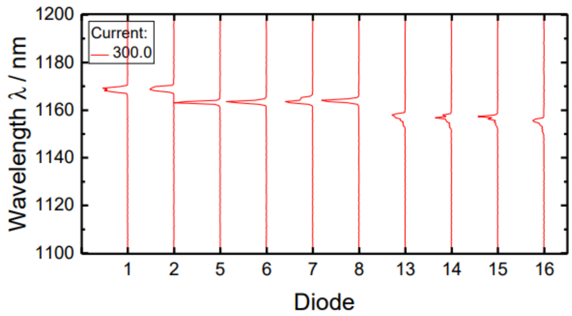

Wafer 4

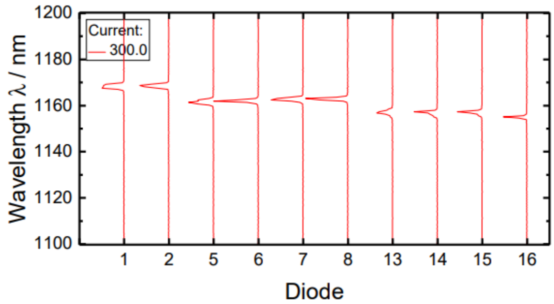

Wafer 5

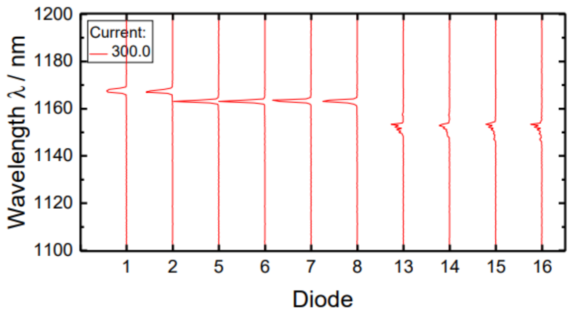

Wafer 6

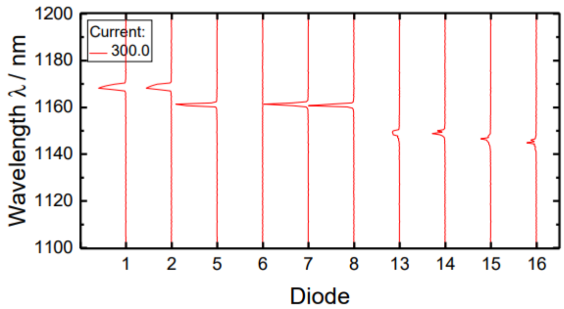

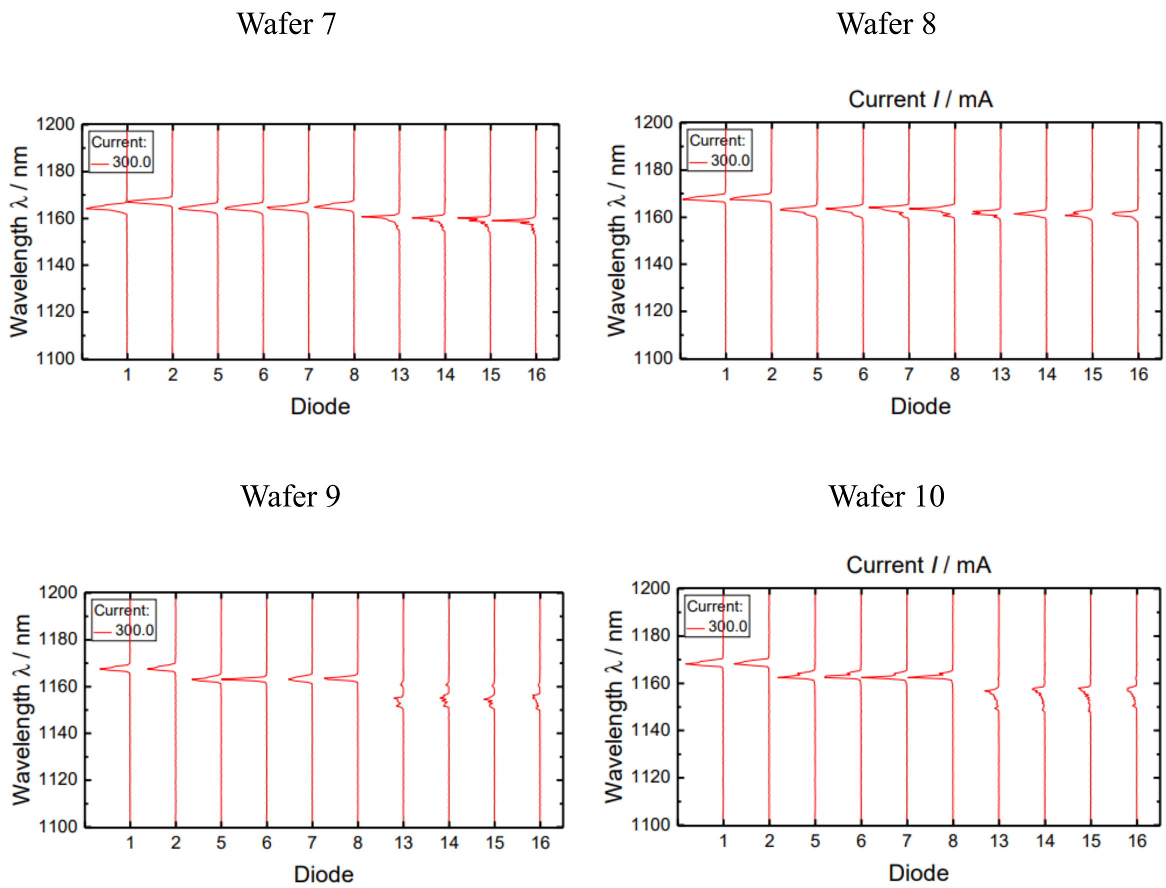

Figure 5.7. Spectrum of emission of the narrow RWG devices 1 to 10.

In each graph, diodes 3 and 4 correspond to LDs with two cleaved facets, diodes 9 to 12 correspond to LDs with one cleaved facet and one etched facet, and diodes 17 to 20 correspond to LDs with two etched facets.

All of the diodes emit light in the infrared wavelength range (1120nm – 1180nm), which fits the emission range on GaAs [11], and a bandwidth of approximately 5nm. The intensity of the peak is higher in those devices showing more vertical profile angles, such as the lasers stemming from the fifth and seventh wafers due to their higher facet reflectivities.

A shift toward lower wavelengths can be observed from the CC LDs to CE LDs to finally EE LDs. This behavior is due to the lower reflectivity of etched facets which leads to higher optical losses and a change in the refraction index. It is this refractive index of the semiconductor which inversely determines the emission wavelengths, as seen in the formulas of section 2.1.3. Therefore, a slight change in wavelength is to be expected.

Now, the output power of the devices at a given current will be illustrated:

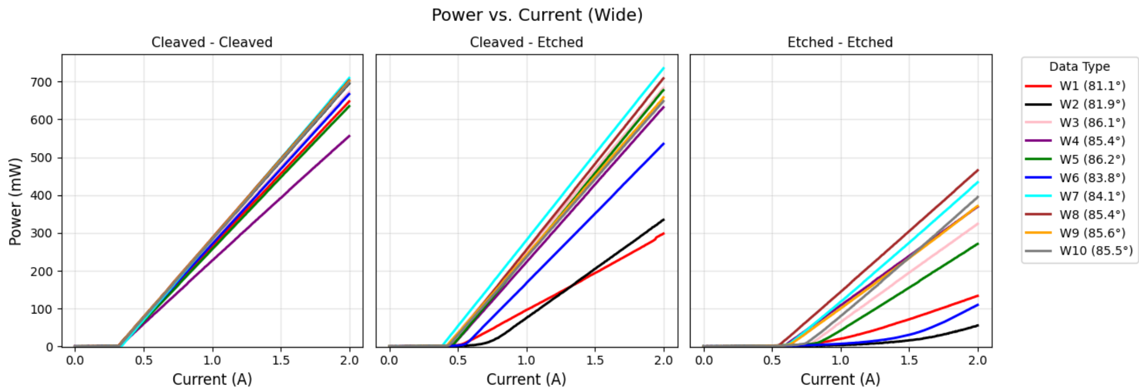

Figure 5.8. Power vs. current curves of the wide RWG lasers.

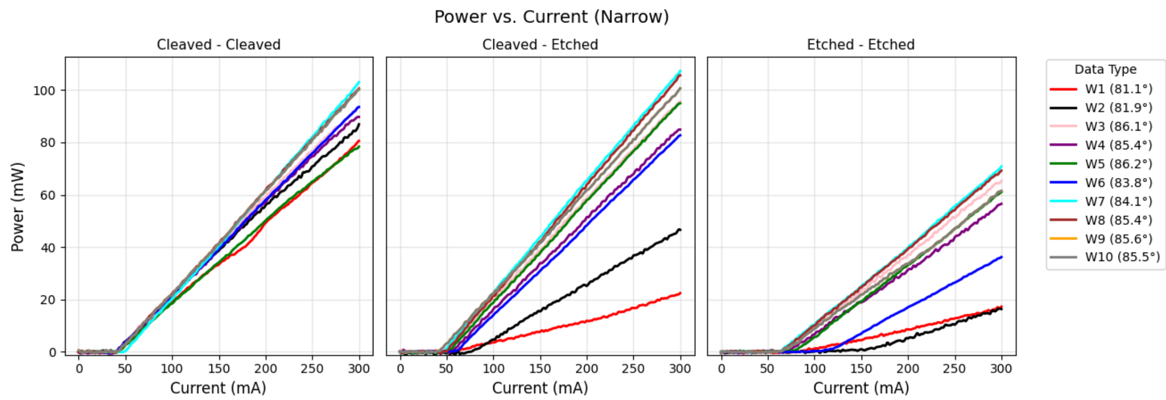

Figure 5.9. Power vs. current curves of the narrow RWG lasers.

As it can be observed in figures 5.8 and 5.9, all devices are functional, showing varying degrees of performance. The measurement range was of 2A for wide lasers and of 300mA for narrow lasers.

The devices with two cleaved facets show almost identical capabilities with slight differences caused by processing. These differences are more visible in the case of the narrow LDs given the reduced power range.

The devices with one cleaved facet and one etched facet start to show major differences. Although some devices offer a similar performance to the LDs with two cleaved facets, namely those with better profile angle, major differences are observed in the rest. For instance, wafer 2 presents a decrease in power of 3 dB and wafer 1, of 6dB.

Finally, LDs with two etched facets show a significant decrease in lasing capabilities, which is to be expected from lower quality facets. Devices with higher vertical profile angles provide the highest powers at the same injected current. Compared to the CC LDs, they show a decrease in power ranging from 2dB (wafer 7) to 7dB (wafer 2).

The most important behavior that can be identified is the shift of the threshold current towards higher current values in LDs with etched facets. That is attributed to the lower reflectivity that facets with lower vertical profile angles offer [38].

The values of I_{th} for each laser were collected:

Wafer	1	2	3	4	5	6	7	8	9	10
I_{th} (A)	0.8	1.1	0.8	0.6	0.75	0.9	0.6	0.56	0.64	0.73
Profile Angle (°)	81,1	81,9	86,1	85,4	86,2	83,8	84,1	85,4	85,6	85,5

Table 8. Threshold current values for the wide RWG lasers with two etched facets.

Wafer	1	2	3	4	5	6	7	8	9	10
I_{th} (mA)	80	160	72	70	82	125	63	62	64	65
Profile Angle (°)	81,1	81,9	86,1	85,4	86,2	83,8	84,1	85,4	85,6	85,5

Table 9. Threshold current values for the narrow RWG lasers with two etched facets.

If the dependance of threshold current on the profile angle of the etched facets is analyzed, the following dependance is obtained:

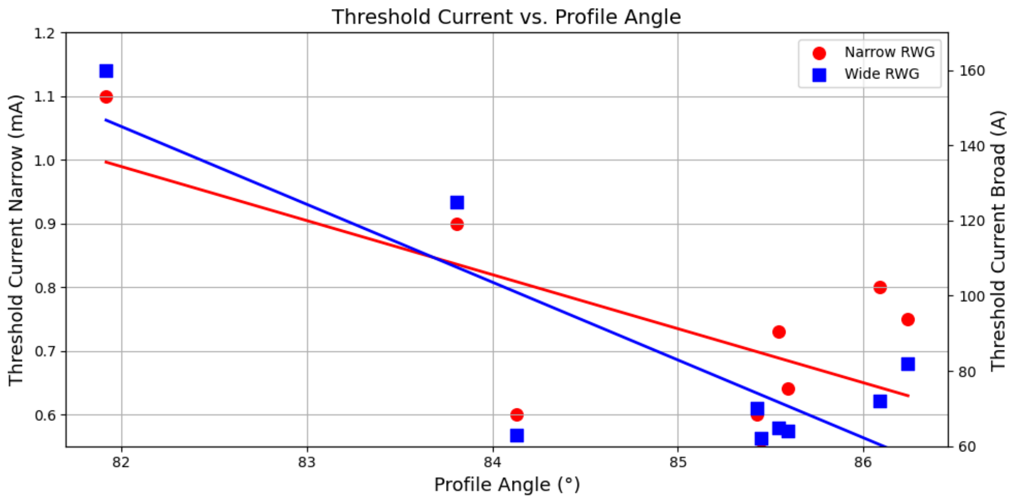

Figure 5.10. Threshold current vs. profile angle of the devices with two etched facets without W1.

As it is to be expected from the theory, a decrease of the threshold current takes place when the facets are more vertical and therefore present a higher reflectivity [6]. Even though the general trend is clear, it seems that other variables could influence the threshold current values too, given the scattered distribution that the points show.

Another variable that is crucial for the characterization of the devices is the slope efficiency (η_s).

The values of η_s for each diode laser were collected:

Wafer	1	2	3	4	5	6	7	8	9	10
η_s (mW/mA)	0.06	0.05	0.22	0.25	0.23	0.05	0.27	0.29	0.24	0.26
Profile Angle (°)	81,1	81,9	86,1	85,4	86,2	83,8	84,1	85,4	85,6	85,5

Table 10. Slope efficiency for the wide-area lasers with two etched facets.

Wafer	1	2	3	4	5	6	7	8	9	10
η_s (mW/mA)	0.07	0.12	0.25	0.23	0.27	0.2	0.29	0.29	0.24	0.28
Profile Angle (°)	81,1	81,9	86,1	85,4	86,2	83,8	84,1	85,4	85,6	85,5

Table 11. Slope efficiency for the narrow RWG lasers with two etched facets.

Based on this data, it was possible to observe a direct relation between slope efficiency and the profile angle:

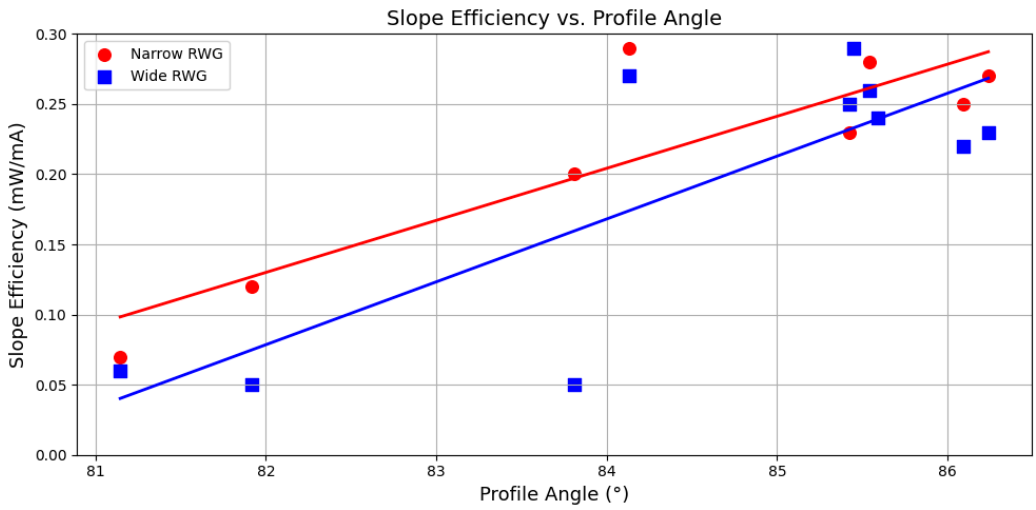

Figure 5.11. Slope efficiency vs. profile angle of the devices with two etched facets.

Following the same logic as with the threshold current, the results are also aligned with the idea that more vertical profile angles lead to higher facet reflectivity and therefore in a more efficient cavity [39].

In figures 5.12 and 5.13, the traces of voltage versus the current are shown for the facet three configurations and RWG width:

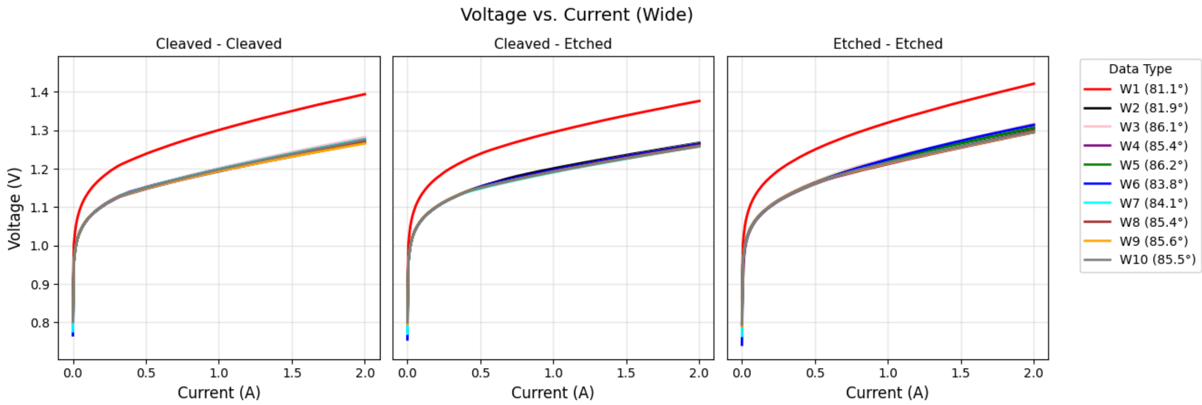

Figure 5.12. Voltage vs. current curves of the wide RWG lasers.

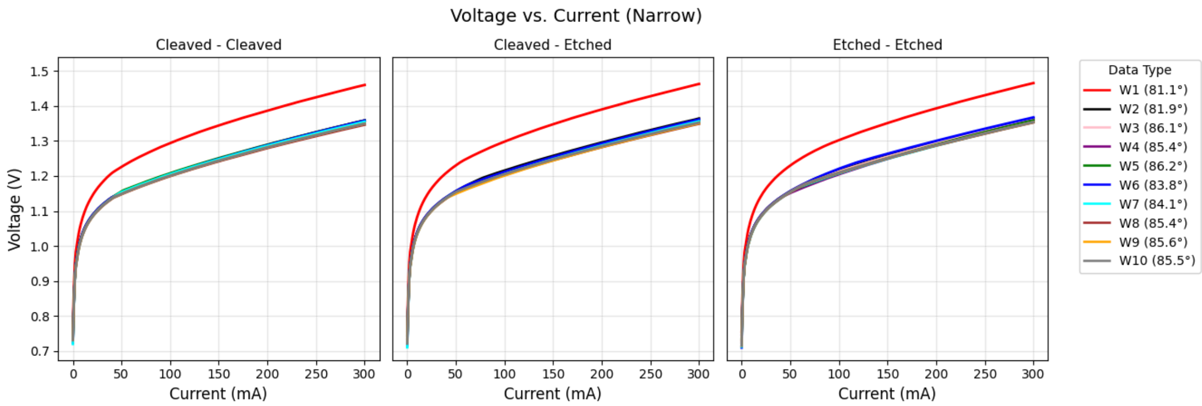

Figure 5.13. Voltage vs. current curves of the narrow RWG lasers.

Even though this parameter is mostly determined by epitaxy and contact quality [40] [41], it still presents a benchmark for performance comparison of the laser diodes. For laser diodes, lower voltage requirements for the devices to emit light are desired.

Devices from wafers 2 to 10 showed a similar performance, given their identical epitaxial structure. However, wafer 1 presents higher voltage values due to its slightly different epitaxial structure. This reinforces the idea that epitaxy is crucial to determine the voltage requirements of laser diodes.

Once again, slight differences between the VI-curves of LDs with wide and narrow RWGs can be observed due to the differences in their RWG surfaces, which resulted in changes in resistivity.

To conclude, both the vertical and lateral farfields of emission were scanned. They provided insight into the emission behavior of the LDs and towards which direction light is emitted through the facets:

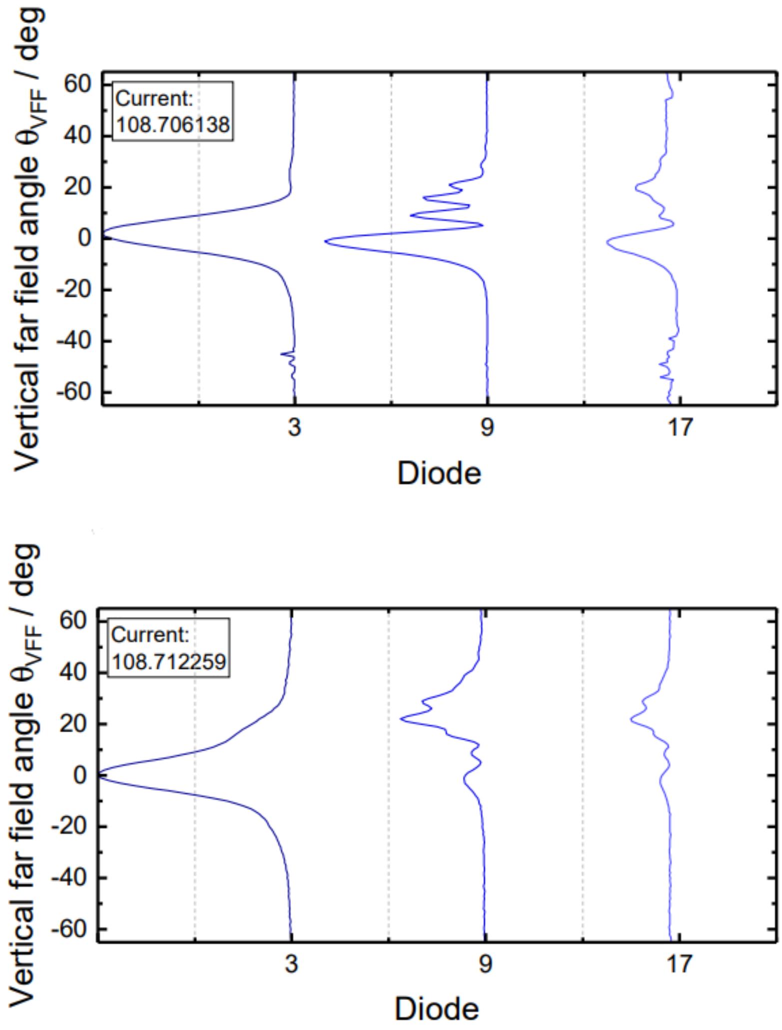

Figure 5.14. Best and worst vertical farfields corresponding to wide RWG LDs from wafer 1 and wafer 4, respectively.

In figure 5.14, diode 3 corresponds to a CC LD, diode 9 corresponds to a CE LD, and diode 17 corresponds to an EE LD. Apart from the evident higher intensity peak in the devices with more vertical profile angle, an upward shift in angle can be observed. That is explained by the fact that light is emitted perpendicularly to the facet. If the facet is not completely vertical, the light beam will be emitted upwards following the perpendicular direction to the facet.

Multiple peaks additional to the main central beam can also be noticed. They are explained by the interference caused by part of the light beam being reflected in the facet trench bottom, as it is illustrated in figure 5.15. The reflected light creates an interference, resulting in several intensity peaks at different angles. This effect is already observed with the introduction of only one etched facet, which is why both configurations with one etched facet and with two etched facets show similar results.

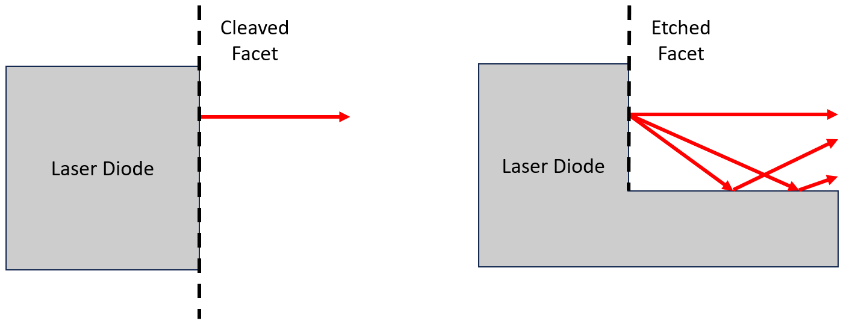

Figure 5.15. Interference comparison in cleaved and etched facets.

Finally, the lateral farfield measurements showed the following results:

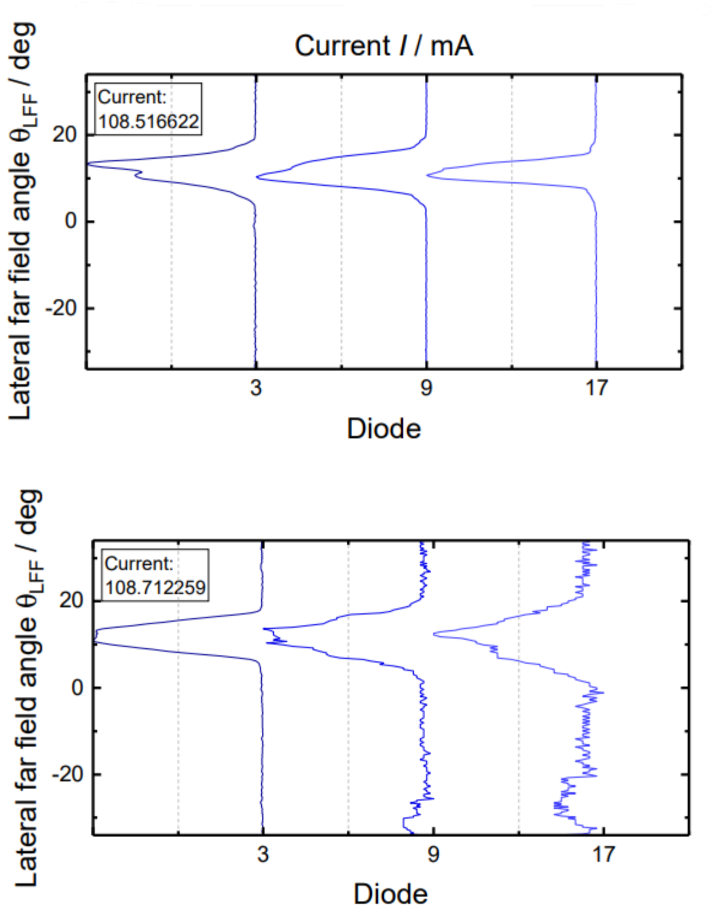

Figure 5.16. Best and worst lateral farfields corresponding to wide RWG LDs from wafer 1 and wafer 4, respectively. The equipment showed an offset of 12°.

In figure 5.16, diode 3 corresponds to a CC LD, diode 9 corresponds to a CE LD, and diode 17 corresponds to an EE LD. In contrast to the vertical farfields, the lateral farfields do not show such remarkable differences as the vertical farfields. Given that profile angles change along the vertical direction, no strong dependance of the profile angles and the lateral fields was expected.

Another undesired effect that could cause lateral light scattering is the formation of the cone-like structures due to contamination micro-masking. As seen in the picture below, the path of the emitted light beam could be altered by their presence in the wafers where the effect took place.

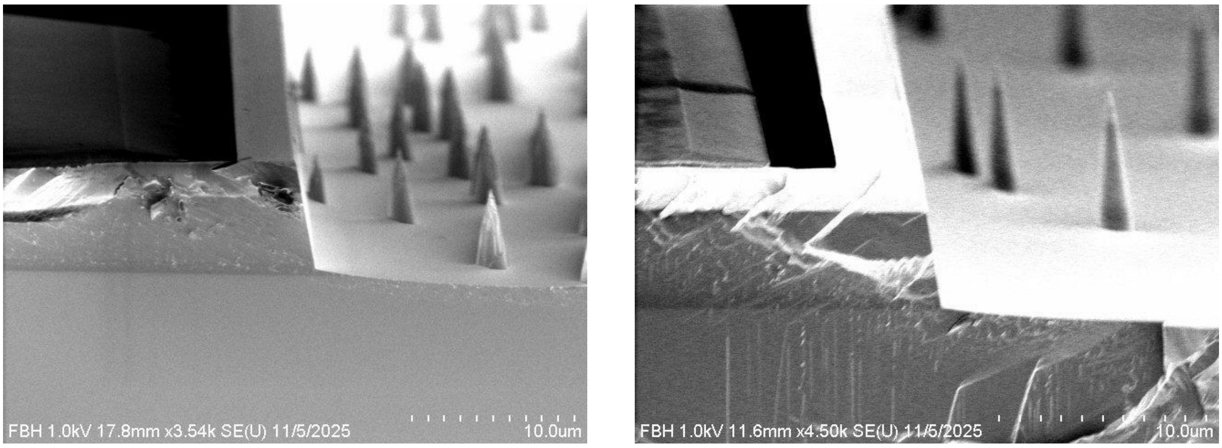

Figure 5.17. Details of devices presenting undesired micro-masking. To the left, wafer 1. To the right, wafer 2.

5.1.4 Final Remarks

The main objective of this work, that is, the demonstration of GaAs-based laser diodes with etched facets, was achieved. To different extents, all devices showed lasing capabilities and emitted light beams when current was injected. The optical measurements allowed for the characterization of the devices and the analysis of what variables and parameters influenced their performance.

The devices offering the best results were:

Device	Wafer	P_{max}	I_{th}	η_s
Wide RWG	8	465mW (I=2A)	0.56A	0.29mW/mA
Narrow RWG	7	72mW (I=300mA)	63mA	0.29mW/mA

Table 12. Best devices with wide and narrow RWG and their characteristics.

The used recipes for the facet etching of wafers were:

Wafer	BCl_3 (sccm)	Cl_2 (sccm)	He (sccm)	N_2 (sccm)	ICP (W)	RF (W)	Pressure (Pa)	Temp. (°C)
7	25	35	10	3	300	100	0.5	25
8	20	40	10	3	300	100	0.5	25

Table 13. Best recipes for facet etching in laser epitaxial wafers.

At the same time, an extensive recipe testing and following variable analysis was carried out, providing valuable insight into what variables have the biggest influence on profile angle, roughness and thus lasing capabilities of the devices. The decrease in pressure, the addition of N_2, and the prevalence of Cl_2 in the gas mix brought the biggest improvements to obtaining more vertical profile angles. The removal of any hard mask during the practical work has also simplified the manufacturing process of the laser diodes without putting their functionality at risk.

Even though there are different aspects that have been overlooked by time constraints or equipment availability, the results of this work are satisfactory and can be of use for future developments in the institute.

5.2 Future Work

Provided that the time for the completion of the project was limited and due to the complexity and high number of processes involved in the creation of the devices, there are many aspects worth of investigation that could not be looked into and would benefit from further experimentation in the future.

First, it is of the utmost importance to complete the design of experiment for recipe testing to involve the modification of variables such as power, temperature, or inert gas flow. The parameter combination for recipe testing can be almost infinite, which is why the project focused on those variables more prone to have an influence in profile angle and facet smoothness based on past results found in the literature.

As the results show, further combinations with higher N2 flows, lower pressures, and higher Cl2 content show the most potential. Nonetheless, in order to obtain the full picture of the physical process and the role that each parameter plays into the final result, the inclusion of additional variable parameters into the design of experiment comes as the natural next step.

Secondly, as exposed in the state of art section, the addition of a wet-etching step after the dry-etching facet etching will help with obtaining more vertical walls, which will accordingly improve final device performance [26]. Only an increase of 1° to 2° would lead to major improvements. Moreover, the coating of the facets with reflective layers would further improve the lasing capabilities of the device by optimizing the resonance of the cavity.

Thirdly, as long as the application allows for it, the use of wafers with a thinner epitaxial structure could improve the final performance and lasing capabilities of the devices, given that a shallower etching step will result in a more controllable and precise process as well as providing less space for impurities and undesired effects to appear. It is always more complex to ensure that a deeper etch will offer accurate repeatability. In this project, wafers with an unusual thick epitaxial structure were used due to availability of materials at the institute, which could be regarded as a worst-case scenario, with most other wafers presenting notably shallower epitaxial structures.

An effect that was overlooked is tailing. As the pictures of the profile shape of the cleaved devices show, the surface of the facet trench bottom is not flat. Instead, it shows an upwards curve when approaching the facet, which often happens in deep etching and is related to the loading effect [36] [37]. Determining how undesired tailing could be mitigated would optimize the facet formation process.

Additionally, now that GaAs wafers have been proved successful in demonstrating functional lasing devices, expanding the range of materials that can be employed for this objective makes sense. Wafers based in compounds such as GaN or InP are already well-established as light sources and adapting this work to these platforms and feasibility studies on whether they can be used for such purposes would enrich research in this field.

Last, more extensive tests on the final devices, such as a stability test over long periods of time, a device performance test with varying temperature environments, or further facet roughness measurement with atomic force microscopy or laser scanning microscopy techniques could both offer further insights into which recipes offer the actual best results taking into account more variables or their suitability for use in real applications as a light source under realistic operating conditions.

6 References

[1] Maiman, T. (1960). *Stimulated optical radiation in ruby*. Nature, 187, 493–494.

[2] Brennan, K. F. (2005). *Introduction to semiconductor devices: For computing and telecommunications applications*. Cambridge University Press.

[3] Singh, S. C., Zeng, H., Guo, C., & Cai, W. (2012). *Lasers: Fundamentals, types, and operations*. In *Nanomaterials: Processing and characterization with lasers* (1st ed.). Wiley-VCH.

[4] Sze, S. M., & Ng, K. K. (2007). *Physics of semiconductor devices* (3rd ed.). Wiley-Interscience.

[5] Wenzel, H., & Zeghuzzi, A. (2017). Chapter 27. In J. Piprek (Ed.), *Handbook of optoelectronic device modeling and simulation: Vol. 2. Lasers, modulators, photodetectors, solar cells, and numerical methods*. CRC Press.

[6] Yuan, L.-D., Deng, H.-X., Li, S.-S., Luo, J.-W., & Wei, S.-H. (2018). *Unified theory of the direct or indirect bandgap nature of conventional semiconductors*. https://doi.org/10.48550/arXiv.1809.05985.

[7] Siew, S. Y., Li, B., Gao, F., Zheng, H. Y., Zhang, W., Guo, P., ... & Lo, G. Q. (2021). Review of silicon photonics technology and platform development. Journal of Lightwave Technology, 39(13), 4374–4389.

[8] Kittel, C., & McEuen, P. (2018). *Introduction to solid state physics*. John Wiley & Sons.

[9] Noffsinger, J., Kioupakis, E., Van de Walle, C. G., Louie, S. G., & Cohen, M. L. (2012). Phonon-assisted optical absorption in silicon from first principles. Physical Review Letters, 108, 167402. https://doi.org/10.1103/PhysRevLett.108.167402

[10] Menéndez, J., Lockwood, D., Zwinkels, J., & Noël, M. (2018). Phonon-assisted optical absorption in germanium. Physical Review B, 98. https://doi.org/10.1103/PhysRevB.98.165207

[11] Sze, S. M. (2008). *Semiconductor devices: Physics and technology*. John Wiley & Sons.

[12] Mason, B., Larson, M., Akulova, Y. A., & Kalluri, S. (2013). InP based photonic integrated circuits for DWDM optical communication. International Conference on Indium Phosphide and Related Materials, 1–2. https://doi.org/10.1109/ICIPRM.2013.6562635

[13] Feyisa, D. W., Shi, B., Kraemer, R., Calabretta, N., & Stabile, R. (2022). Compact 8×8 SOA-based optical WDM space switch in generic InP technology. Journal of Lightwave Technology, 40(19), 6331–6338.

[14] Singer, S., et al. (2024). LiDAR demonstration using an InP optical phased array (OPA) with a 3D-printed optical beam-shaping element. ECOC 2024: 50th European Conference on Optical Communication, 1635–1638.

[15] Iucolano, F., & Boles, T. (2019). GaN-on-Si HEMTs for wireless base stations. *Materials Science in Semiconductor Processing, 98*, 100–105.

[16] Pearton, S. J., et al. (2016). *ECS Journal of Solid State Science and Technology, 5*, Q35.

[17] Esame, O., Gurbuz, Y., Tekin, I., & Bozkurt, A. (2004). Performance comparison of state-of-the-art HBT devices based on AlGaAs/GaAs, Si/SiGe and InGaAs/InP. *Microelectronics Journal, 35*(11), 901–908.

[18] Khabibullin, R. A., Vasil'evskii, I. S., Galiev, G. B., et al. (2011). Effect of the built-in electric field on optical and electrical properties of AlGaAs/InGaAs/GaAs P-HEMT nanoheterostructures. *Semiconductors, 45*, 657–662.

[19] Lieberman, M. A., & Lichtenberg, A. J. (1994). *Principles of plasma discharges and materials processing*. MRS Bulletin, 30(12), 899–901.

[20] Nojiri, K. (2015). *Dry etching technology for semiconductors* (pp. 1–116). Springer.

[21] Sugawara, M. (1998). *Plasma etching: Fundamentals and applications* (Vol. 7). OUP Oxford.

[22] Dobkin, D., & Zuraw, M. K. (2003). *Principles of chemical vapor deposition*. Springer.

[23] Gibasiewicz, K., Kafar, A., Schiavon, D., Saba, K., Marona, Ł., Kamińska, E., & Perlin, P. (2023). InGaN laser diodes with etched facets for photonic integrated circuit applications. *Micromachines, 14*, 408.

[24] Hu, D., Zhang, C., Meissner, T., Liu, Y., & Klamkin, J. (2025). Quantum dot lasers with etched facets and waveguide turns for silicon photonics integration. In *Advanced Photonics Congress* (paper ITh3B.4). Optica Publishing Group.

[25] Genc, M., Zubialevich, V. Z., Hazarika, A., Parbrook, P. J., Corbett, B., & Li, Z. (2023). Continuous-wave operation of 457 nm InGaN laser diodes with etched facet mirrors for on-chip photonics. *Advanced Photonics Research, 4*, 2300208.

[26] Huang, Z., Zimmer, M., Hepp, S., Jetter, M., & Michler, P. (2019). Optical gain and lasing properties of InP/AlGaInP quantum-dot laser diode emitting at 660 nm. *IEEE Journal of Quantum Electronics, 55*(2), Article 2000307.

[27] Park, Y. H., Kim, J. K., Lee, J. H., Joo, Y. W., Noh, H. S., Lee, J. W., & Pearton, S. J. (2010). N_2 effect on GaAs etching at 150 mTorr capacitively coupled Cl_2/N_2 plasma. *Microelectronic Engineering, 87*(4), 548–552.

[28] Vigneron, P. B., Joint, F., Isac, N., Colombelli, R., & Herth, E. (2018). Advanced and reliable GaAs/AlGaAs ICP-DRIE etching for optoelectronic, microelectronic and microsystem applications. *Microelectronic Engineering, 202*, 42–50.

[29] Hays, D. (1999). *Selective etching of compound semiconductors*.

[30] McLane, G. F., & Buchwald, W. R. (1994). Dry etch–induced defects and H passivation of GaAs surfaces produced by CH_4/H_2/Ar plasmas. *MRS Proceedings, 340*, 221.

[31] Stareev, G. (1993). Formation of extremely low resistance Ti/Pt/Au ohmic contacts to p-GaAs. *Applied Physics Letters, 62*(22), 2801–2803.

[32] Crouch, M. A., Gill, S. S., Woodward, J., Courtney, S. J., Williams, G. M., & Cullis, A. G. (1990). Structure and electrical properties of Ge/Au ohmic contacts to n-type GaAs formed by rapid thermal annealing. *Solid-State Electronics, 33*(11), 1437–1446.

[33] Lee, Y. H., Sung, Y. J., Yeom, G. Y., Lee, J. W., & Kim, T. I. (2000). Magnetized inductively coupled plasma etching of GaN in Cl_2/BCl_3 plasmas. *Journal of Vacuum Science & Technology A, 18*(4), 1390–1394.

[34] Shul, R. J., Zhang, L., Willison, C. G., Han, J., Pearton, S. J., Hong, J., … Lester, L. F. (1998). Group-III nitride etch selectivity in BCl_3/Cl_2 ICP plasmas. MRS Proceedings, 537, G8.1. https://doi.org/10.1557/PROC-537-G8

[35] Tuda, M., Nishikawa, K., & Ono, K. (1997). Numerical study of the etch anisotropy in low-pressure, high-density plasma etching. *Journal of Applied Physics, 81*(2), 960–967.

[36] Min, J. H., Hwang, S. W., Lee, G. R., & Moon, S. H. (2003). Redeposition of etch products on sidewalls during SiO_2 etching in a CF_4 plasma. III. Effects of O_2 addition to CF_4 plasma. *Journal of Vacuum Science & Technology B, 21*, 1210.

[37] Nakazaki, N., Tsuda, H., Takao, Y., Eriguchi, K., & Ono, K. (2014). Two modes of surface roughening during plasma etching of silicon: Role of ionized etch products. *Journal of Applied Physics, 116*(22).

[38] Gillgrass, S. J. (2018). *Laser haemocytometer* (PhD thesis). Cardiff University.

[39] Burman, T. T., Cao, Z., Allford, C., Baker, J., Patel, J., Ashraf, H., ... & Smowton, P. M. (2024). Assessing plasma-etched InP laser facet quality. *IEEE Photonics Technology Letters, 36*(11), 745–748.

[40] Lin, T., Xie, J. N., Ning, S. H., Li, Q. M., & Li, B. (2021). Study on the p-type ohmic contact in GaAs-based laser diode. *Materials Science in Semiconductor Processing, 124*, 105622.

[41] Hantschmann, C., Liu, Z., Tang, M., Chen, S., Seeds, A. J., Liu, H., ... & Penty, R. V. (2020). Theoretical study on the effects of dislocations in monolithic III–V lasers on silicon. *Journal of Lightwave Technology, 38*(17), 4801–4807.

7 List of Tables

Table 1. III-V compounds used for laser diodes and their applications.

Table 2. Recipe parameters used for standard RWG etching.

Table 3. Recipe experiment table for facet etching on wafer quarters.

Table 4. Best recipes from the tests and initial recipes for facet etching in laser epitaxial wafers.

Table 5. RWG height measured in laser epitaxial wafers.

Table 6. Recipes for facet etching in laser epitaxial wafers.

Table 7. Average values of the achieved profile angles.

Table 8. Threshold current values for the wide RWG lasers.

Table 9. Threshold current values for the narrow RWG lasers.

Table 10. Slope efficiency for the wide-area lasers with two etched facets.

Table 11. Slope efficiency for the narrow RWG lasers with two etched facets.

Table 12. Best devices with wide and narrow RWG and their characteristics.

Table 13. Best recipes for facet etching in laser epitaxial wafers.

8 List of Figures

Figure 2.1 Depiction of the a) absorption, b) stimulated emission, and c) spontaneous emission by a two-level atom that presents two energy states E1 and E2 with a luminescence lifetime of T2.

[1] Pollnau, Markus. (2019). Are absorption and spontaneous or stimulated emission inverse processes? The answer is subtle! Applied Physics B. 125. 10.1007/s00340-019-7133-z.

Figure 2.2. Schematic of the epitaxial laser epitaxy of the wafers.

Figure 2.3 Direct bandgap vs. indirect bandgap schemes in the k-space with a given Fermi level (e_F) and wave number (k_F).

[2] Abedin, Minhaz. (2015). A self-adjusting lin-log active pixel for wide dynamic range CMOS image sensor. 10.13140/RG.2.1.3871.8965.

Figure 2.4 Emission spectrum of laser diodes based on different III-V compounds.

Figure 2.5 Variation of the refractive index of $Al_xGa_{1-x}As$ vs. the fraction of Al(x).

Figure 2.6 Comparison of anisotropic etching (to the left) vs. isotropic etching (to the right).

Figure 2.7 Schematics of an ICP-RIE equipment.

[3] Valerio Flavio Gili. All-dielectric nonlinear nanophotonics. Material chemistry. Université Sorbonne Paris Cité, 2018. English.

Figure 2.8 View of the simulation software tool for computing refractivity periods. Epitaxial structure of the wafers to the left and the period representation to the right.

Figure 3.1 Schematic of the proposed laser diode structure indicating the elements of the device.

Figure 4.1 SEM inspections from wafer 5 and 6 after the ridged waveguide etching was performed.

Figure 4.2 SEM inspection of facet detail from recipes 17 and 19. Redeposition-caused crest next to the facet to the left. Correctly facet etching to the right.

Figure 4.3 Optical microscope inspections of the RWGs of wafer 11 at 5x and 100x from wafer 10 after CVD was performed.

Figure 4.4 Optical microscope inspections at 5x from wafer 10 before, showing part of the Si_3N_4 CVD layer, and after the etching, with no traces of visible Si_3N_4.

Figure 4.5 SEM inspections of wafer 7 after the K1 layer etch was performed. The RWG pattern was incorrectly etched into the wafer.

Figure 4.6 AlGaAs etch rate comparison obtained using a photoresist mask and hard mask.

Figure 4.7 SEM inspection of wafer 7 showing poor facet formation when using a hard mask. The facet edge is in the vertical direction.

Figure 4.8 Etch rate and selectivity comparison between the recipes used with photoresist mask.

Figure 4.9 Etch rate comparison obtained with CH4/Cl2 gas mix at different pressures.

Figure 4.10 Schematic of the epitaxial structure of the wafers with the depth of the two etching steps.

Figure 4.11 Old and new reticle approach for the RWG design, respectively.

Figure 4.12 Visual flow of the 6-layer full device process for the diode lasers.

Figure 4.13 Reflectivity period simulation for a 1.5µm etch in a 950nm wavelength.

Figure 4.14 K-Layer details of wafer 4 inspected in an optical microscope. To the left, control structures of the layer. To the right, zoomed-in view of the new RWG design.

Figure 4.15 I-Layer details of wafer 1 inspected in an optical microscope before the etch. To the left, wide 5x overview of lasing devices and wafer numbering. To the right, 100x detailed view of facets.

Figure 4.16 I-Layer details of wafer 1 inspected in an optical microscope after the etch. To the left, wide 5x overview of lasing devices and wafer numbering. To the right, 100x detailed view of facets.

Figure 4.17 I-Layer details of wafer 1 inspected in SEM after the etching, showing surface coverage except for contacts and facet openings.

Figure 4.18 M-Layer optical inspection of wafer 1 showing the individual devices and their identification number before and after contact metal deposition.

Figure 4.19 Reflectivity periods of the epitaxial structure at 488nm, 633nm, and 950nm, respectively.

Figure 4.20 K1-Layer optical inspection of wafer 1 after lithography.

Figure 4.21 K1-Layer SEM inspection of wafer 1 after facet etching.

Figure 4.22 K1-Layer SEM inspection of wafer 5 after NH_4OH/H_2O cleaning and facet etching.

Figure 4.23 Measurement of a facet of wafer 2 width with SEM.

Figure 4.24 Top mapping of wafer 1with the optical microscope before cleaving.

Figure 4.25 Top view of the cleaved devices after cleaving.

Figure 4.26 Measurement station where the results were obtained. Measurement station where the results were obtained, showing the device holder, the top-view microscope, and the measurement devices.

Figure 4.27 Detailed view of the device under testing before and during contact. Only two of the four needles are places on the device under test.

Figure 5.1 Influence of the pressure on the profile angle with different BCl_3/Cl_2 ratios.

Figure 5.2 Influence of the BCl_3/Cl_2 ratio on the profile angle at different pressure values.

Figure 5.3 Influence of the N_2 flux on the profile angle.

Figure 5.4 Vertical view of the undesired structures due to contamination masking. To the left, wafer 2. To the right, wafer 9.

Figure 5.5 Measurements of profile angle after cleaving the devices. To the left, wafer 2. To the right, wafer 5.

Figure 5.6 Undesired tailing taking place at the bottom of the facet trench. To the left, wafer 8. To the right, wafer 10.

Figure 5.7 Spectrum of emission of the narrow RWG devices 1 to 10.

Figure 5.8 Power vs. current curves of the wide RWG lasers.

Figure 5.9 Power vs. current curves of the narrow RWG lasers.

Figure 5.10 Threshold current vs. profile angle of the devices with two etched facets without W1.

Figure 5.11 Slope efficiency vs. profile angle of the devices with two etched facets.

Figure 5.12 Voltage vs. current curves of the wide RWG lasers.

Figure 5.13 Voltage vs. current curves of the narrow RWG lasers.

Figure 5.14 Best and worst vertical farfields corresponding to wide RWG LDs from wafer 1 and wafer 4, respectively.

Figure 5.15. Interference comparison in cleaved and etched facets.

Figure 5.16 Best and worst lateral farfields corresponding to wide RWG LDs from wafer 1 and wafer 4, respectively. The measuring equipment shows an offset error of approximately 13°.

Figure 5.17 Details of devices presenting undesired micro-masking. To the left, wafer 1. To the right, wafer 2.

9 ABBREVIATIONS

1. µTP: Micro-Transfer Printing.
2. HBT: Heterojunction Bipolar Transistor.
3. MOSFET: Metal-Oxide-Semiconductor Field-Effect Transistor.
4. LED: Light-Emitting Diode.
5. DFB: Distributed Feedback Laser.
6. LD: Laser Diode.
7. VCSEL: Vertical-Cavity Surface-Emitting Laser.
8. PCSEL: Photonic Crystal Surface-Emitting Laser.
9. DWDM: Dense Wavelength-Division Multiplexing.
10. HEMT: High-Electron-Mobility Transistor.
11. RF: Radiofrequency.
12. DC: Direct Current.
13. RIE: Reactive-Ion Etching.
14. ICP: Inductively-Coupled Plasma.
15. CCP: Capacitively-Coupled Plasma.
16. CVD: Chemical Vapor Deposition.
17. TCVD: Thermal Chemical Vapor Deposition.
18. LPCVD: Low-Pressure Chemical Vapor Deposition.
19. PECVD: Plasma-Enhanced Chemical Vapor Deposition.
20. MOCVD: Metal-Organic Chemical Vapor Deposition.
21. APCVD: Atmospheric Pressure Chemical Vapor Deposition.
22. ALD: Atomic Layer Deposition.
23. TALD: Thermal Atomic Layer Deposition.
24. PEALD: Plasma-Enhanced Atomic Layer Deposition.
25. RWG: Ridged Waveguide.
26. PIC: Photonic Integrated Circuit.
27. MTP: Micro-Transfer Printing.
28. DOE: Design of Experiment.
29. SEM: Scanning Electron Microscope.

30. AFM: Atomic Force Microscope.
31. CC, CE, EE: Cleaved-Cleaved, Cleaved-Etched, Etched-Etched.

10 ACKNOWLEDGEMENTS

To conclude this work,

I would like to thank Dr. Olaf Krüger, for offering me the amazing opportunity of working at FBH.

I would like to thank my supervisors Dr. Ralph Stefan-Unger and Dr. Dominik Martin for their guidance, advice, and patience during these six months.

I would like to thank the Optoelektronik Abteilung, who provided the necessary materials to carry out this work.

I would like to thank the Prozesstechnologie Abteilung, who have taught me how to make use of the equipment and have been involved in many steps of the front-end processing.

Vielen Dank.